Chemie der Erde 77 (2017) 53–67

Contents lists available at ScienceDirect

Chemie der Erde

journal homepage: www.elsevier.de/chemer

# Geology, geochemistry and petrogenesis of post-collisional adakitic intrusions and related dikes in the Khoynarood area, NW Iran

Hossein Mahmoudi Nia [a], Saeid Baghban [a], Vartan Simmonds [b,*]

[a] Earth Sciences Department, Faculty of Natural Sciences, University of Tabriz, 5166616471, Tabriz, Iran
[b] Research Institute for Fundamental Sciences, University of Tabriz, 5166616471, Tabriz, Iran

ARTICLE INFO

*Article history:*
Received 20 August 2016
Received in revised form
24 December 2016
Accepted 14 February 2017
Editorial handling - Hadi Shafaii Moghadam

*Keywords:*
Khoynarood
High-silica adakite
Subducting oceanic crust
Neo-Tethys
Oceanic crust break-off

ABSTRACT

The Khoynarood area is located in the northwest of Iran, lying at the northwestern end of the Urumieh–Dokhtar volcano-plutonic belt and being part of the Qaradagh–South Armenia domain. The main intrusive rocks outcropped in the area have compositions ranging from monzonite–quartz monzonite, through granodiorite, to diorite–hornblende diorite, accompanied by several dikes of diorite–quartz diorite and hornblende diorite compositions, which were geochemically studied in order to provide further data and evidence for the geodynamic setting of the region. The $SiO_2$, $Al_2O_3$ and MgO contents of these rocks are about 58.32–68.12%, 14.13–18.65% and 0.68–4.27%, respectively. They are characterized by the $K_2O/Na_2O$ ratio of 0.26–0.58, $Fe_2O_3 + MnO + MgO + TiO_2$ content about 4.27–13.13%, low Y (8–17 ppm) and HREE (e.g., 1–2 ppm Yb) and high Sr contents (750–1330 ppm), as well as high ratios of Ba/La (13.51–50.96), $(La/Yb)_N$ (7–22), Sr/Y (57.56–166.25), Rb/La (1.13–2.96) and La/Yb (10–33.63), which may testify to the adakitic nature of these intrusions. Their chemical composition corresponds to high-silica adakites, displaying enrichments of LREEs and LILEs and preferential depletion of HFSEs, (e.g., Ti, Ta and Nb). The REE differentiation pattern and the low HREE and Y contents might be resulted from the presence of garnet and amphibole in the solid residue of the source rock, while the high Sr content and the negative anomalies of Ti, Ta and Nb may indicate the absence of plagioclase and presence of Fe and Ti oxides in it. As a general scenario, it may be concluded that the adakitic rocks in the Khoynarood were most likely resulted from detachment of the subducting Neo-Tethyan eclogitic slab after subduction cessation between Arabian and Central Iranian plates during the upper Cretaceous–early Cenozoic and partial melting of the detached slab, followed by interactions with metasomatized mantle wedge peridotite and contamination with continental crust.



## 1. Introduction

Adakites are silica-rich magmatic rocks with high Sr/Y and La/Yb ratios, which are commonly found in different tectonic settings, such as subduction and continental collision zones (Defant and Drummond, 1990; Guo et al., 2007). Adakites are distinguished from boninites by LREE enrichment (La/Yb >40), high Sr content (>400 ppm), high Sr/Y and low $^{87}Sr/^{86}Sr$ ratios, and low radiogenic and non-radiogenic Pb concentrations (Defant and Drummond, 1990; Grove et al., 2005). Adakites were initially believed to be related to the convergent plate margins formed through the melting of hot and young oceanic crusts (<25 Ma; Kay, 1978; Defant and Drummond, 1990; Green and Harry, 1999). However, other genetic models have also been proposed for adakites, including partial melting of mantle wedge materials (e.g., Castillo et al., 1999; Robin et al., 2009) or thickened and/or delaminated garnet-bearing mafic lower crust, underplating of basaltic magmas under a thick continental crust (e.g., Atherton and Petford, 1993; Barnes et al., 1996), high-pressure fractionation (involving garnet) of a hydrous basaltic magma (e.g., Prouteau and Scaillet, 2003; Macpherson et al., 2006) and mixing of basaltic magmas with felsic melts derived from continental crust in both arc and non-arc tectonic settings (Guo et al., 2007). Adakitic rocks are also reported from young island arcs, as well as post-collisional regions (e.g., Jahangiri, 2007 and Simmonds, 2013 from NW Iran). Owing to their particular and characteristic composition, adakites can reflect their source condition and tectonic setting.

Martin et al. (2005) have classified adakites into 2 groups of low-silica (LSA) and high-silica (HSA). HSAs are formed through melting

* Corresponding author at: Research Institute for Fundamental Sciences, University of Tabriz, 5166616471, Tabriz, Iran.
*E-mail addresses:* simmonds_vartan@tabrizu.ac.ir, simmonds_vartan@yahoo.co.uk (V. Simmonds).

http://dx.doi.org/10.1016/j.chemer.2017.02.001
0009-2819/

of the subducted metabasaltic oceanic slab in the stability field of garnet, while LSAs are generated from partial melting of the garnet-bearing metasomatized mantle wedge. Another group of adakites is also introduced, known as continental or potassic adakites, which are resulted from various petrogenetic processes (Rapp et al., 2002; Ding et al., 2007; Gao et al., 2007; Wang et al., 2007a; Wang et al., 2007b).

In many cases, adakitic composition can indicate high-pressure melting of a mafic source, with a garnet-bearing residue left behind (leading to low HREE and Y) but no residual plagioclase (high Sr content). However, medium-pressure melting of garnet-bearing pelitic rocks also provides high La/Yb ratio which, in such cases, cannot be considered as adakitic geochemical characteristics (Moyen, 2009). Moreover, the continental crust melting and fractionation processes also lead to generation of adakitic composition (Macpherson et al., 2006).

The Khoynarood area is located 120 km north of Tabriz. This area is part of the Qaradagh mountain range and Alpine orogenic belt. Several intrusions of Oligocene age have intruded into the upper Cretaceous–Paleocene flyschoid rocks in this area. Their compositions range from monzonite–quartz monzonite through granodiorite to diorite.

According to Brunet et al. (2003), the study area is located in the South Armenia–Qaradagh zone and based on authors such as Nabavi (1976), it is part of the Alborz Azarbaidjan zone in NW Iran. It lies on the Urumieh–Dokhtar Tertiary volcano-plutonic belt (UDMA) at its NW section (Fig. 1a), neighboring the Qaradagh batholith in NW Iran and Meghri-Ordubad pluton in the southern Lesser Caucasus. This magmatic belt with 2000 km length and 50 km width was formed by the subduction of the Neo-Tethyan oceanic crust. It extends to the Lesser Caucasus and East Turkey (Lustrino et al., 2010, 2012) and contains volcanic and plutonic rocks of the Eocene and post-Eocene ages.

The time of closure and the evolution history of the Neo-Tethys Ocean in Iranian domain are still matters of controversy (Aghanabati, 2004). These uncertainties have led different authors to suggest various theories for the evolution of the Neo-Tethys basin. Authors like Berberian and King (1981), Mohajjel and Fergusson (2000), Agard et al. (2005) and Ghasemi and Talbot (2006) propose a single-stage subduction scenario for the Neo-Tethyan oceanic crust beneath Central Iran, attributing the compositional variations in UDMA rocks to the subduction angle or even the detachment of the subducting slab (slab break-off) during the Eocene and Miocene (Agard et al., 2005), whereas Amidi et al. (1984) believe that the UDMA has a post-collisional nature.

Contrastingly, Glennie (2000) advocates a double-stage subduction for the Neo-Tethys (I and II), considering the opening of two parallel ocean basins. Recent studies show that the collision between Arabian and Central Iranian blocks occurred in the early Cenozoic (Ghasemi and Talbot, 2006; Horton et al., 2008). However, based on the clastic zircon dating from the north of Central Iranian domain, Horton et al. (2008) have placed the collision date of Arabian and Central Iranian plates between middle Eocene and late Oligocene, whereas other geologists propose different dates: late-Cretaceous to early-Paleocene (Ghalamghash et al., 2009; Mazhari et al., 2009), late Paleocene (Agard et al., 2005) and middle to late-Miocene (Azizi and Moinevaziri, 2009).

Several adakitic occurrences have been reported from different parts of UDMA (Jahangiri, 2007; Omrani et al., 2008; Aghazadeh et al., 2011; Simmonds, 2013; Pang et al., 2016), along with reports of ultra-potassic and alkaline basic magmatism of the late Miocene and Plio–Quaternary age, which post-dates the adakitic occurrences (e.g., Jahangiri, 2007; Jahangiri et al., 2011; Aghazadeh et al., 2010; Shafaii Moghadam et al., 2014). In this regard, the intrusive bodies in Khoynarood were subjected to detailed geochemical studies to compare them with other studied intrusions in the region and provide additional data basis to support the geodynamic scenario proposed for the region, as investigating the different parts of UDMA can help to elucidate the uncertainties related to the subduction history of the Neo-Tethyan oceanic crust beneath the Central Iran, the fate of the subducting slab and the time of the collision.

## 2. Geology of the study area

An oval-shape intrusive body of monzonite–quartz monzonite composition (with relative age of Oligocene, considering the history of magmatism in the region and the age of neighboring dated intrusive bodies, as well as the cross-cutting and stratigraphic relationship with respect to the country rocks) intruded the upper Cretaceous–Paleocene flyschoids (Figs. 1 b and 2 ). It subsequently suffered argillic and propylitic alterations. Flyschoid sediments have been precipitated in an environment with high subsidence, probably corresponding to a pull-apart basin. They include alternations of limestone, sandy limestone, shale (containing *Globotruncana* and *Heterohelix* microfossils) and submarine tuff (with traces of *Rotalia*) (Mehrpartou et al., 1992). Due to the presence of extensional conditions during the formation of such a basin, submarine basic magmatism accompanies these sediments. Accordingly, basaltic and andesi-basaltic lavas are alternatively observed in the northern parts of the host flyschoid association which, based on microscopic studies, show hyalomicrolitic porphyritic and microlitic porphyritic textures and moderate to intense propylitic alteration. They are composed of clinopyroxene and plagioclase phenocrysts, set in a highly chloritized and epidotized, vitric and fine-grained groundmass. For the study region, such a pull-apart basin was most likely related to the dip-angle subduction of the Neo-Tethyan oceanic crust in NW Iran (e.g. Saccani et al., 2013; Hajialioghli and Moazzen, 2014), which was subsequently closed following the closure of the Neo-Tethys.

According to the field studies, a porphyritic diorite stock intruded the monzonite–quartz monzonite body within which, epithermal gold-bearing cross-cutting silicic veins have been developed. In this regard, it post-dates the porphyritic monzonite body, while it is older than the epithermal mineralization. The presence of xenoliths from monzonitic stock within the porphyritic diorite confirms the suggested sequence. There are also dioritic dikes, similar in composition to the dioritic stock, which cross-cut the monzonitic body and seem to be branched off from the dioritic stock. The porphyritic hornblende-diorite body and the related dikes in the western part of the study area also show distinct contact and cross-cutting relationship with the porphyritic diorite stock.

Granodioritic body is bright-color and has genetic relationship with the rest of the intrusive rocks in the area, being ascended from a common magma chamber and post-dating the other intrusive bodies (Fig. 1b). All these bodies and the related dikes form a multi-episode intrusive complex. They emplaced within the upper Cretaceous–Paleocene flyschoids, producing contact metamorphism in albite–epidote–hornfels facies, as well as vast hydrothermal alterations in the area, including phyllic, argillic and propylitic alterations. Due to the presence of abundant quartz in the argillic alteration zone, protruded outcrops of quartz can be found in this zone.

## 3. Materials and methods

Following the detailed field survey in the study area, a total of 60 rock samples were collected from the magmatic bodies to carry out petrographic and whole-rock geochemical studies. Petrographic studies were performed using an Olympus BX60 polarized light microscope at the Petrology laboratory, University of Tabriz.

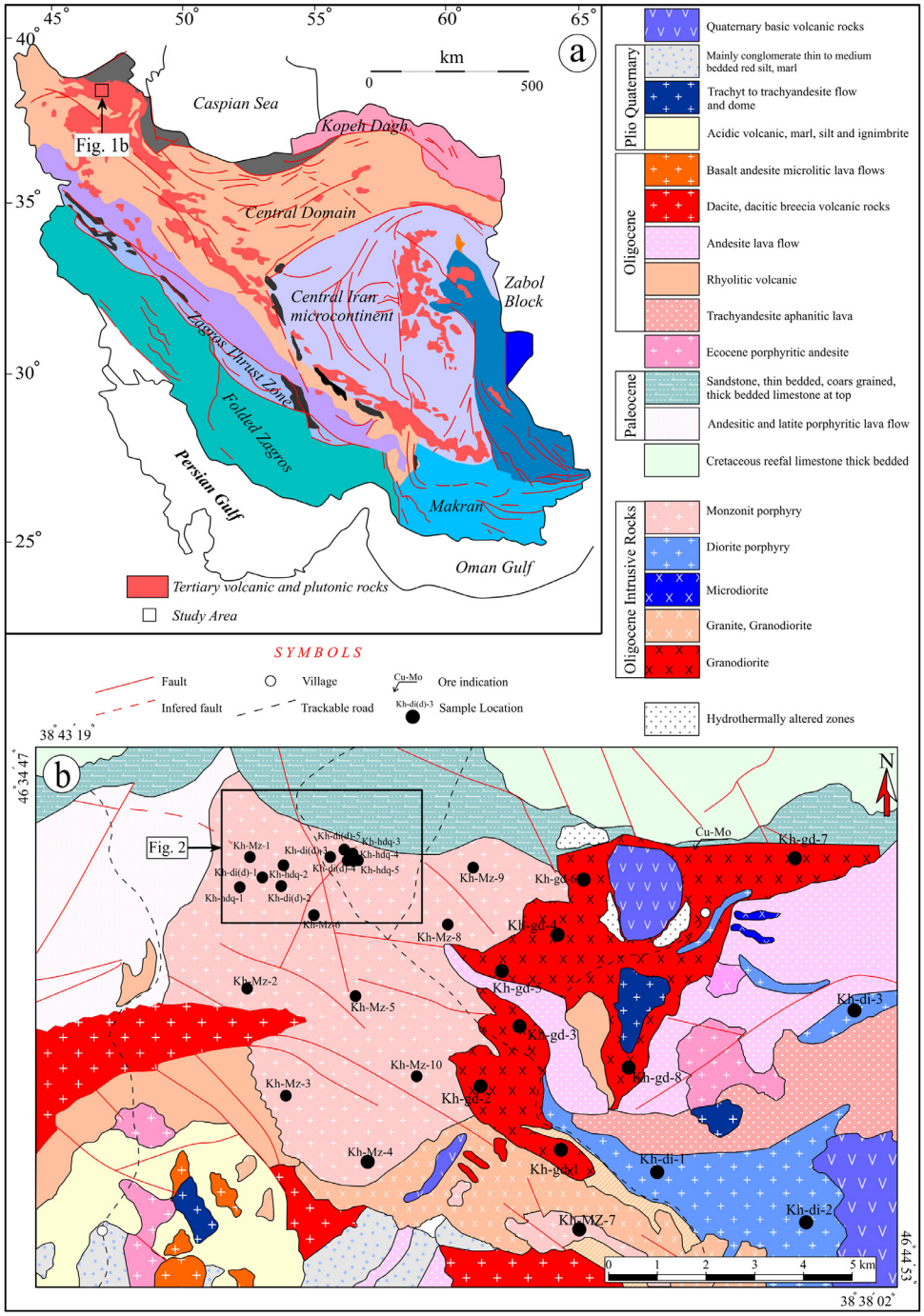


**Fig. 1.** (a) Tectonic and structural map of Iran (Aghanabati, 2004). The location of the study area is shown by a quadrangle. The Urumieh–Dokhtar magmatic arc is recognizable as NW–SE-trending Tertiary volcanic and plutonic rocks, parallel to the Neo-Tethys suture zone. (b) Regional geological map of the Khoynarood area, showing the occurrence and distribution of various plutonic and volcanic units (modified after Mehrpartou et al., 1992). The location of studied samples are shown on the map.

From the studied samples, 30 least altered samples were selected to be analyzed by X-Ray Fluorescence Spectroscopy (XRF) for major oxides and Inductively Coupled Plasma Mass Spectrometry (ICP-MS) for trace and rare earth elements at ALS-Chemex Lab (Canada). Samples were cut by a diamond-bonded brass saw blade, crushed in a steel jaw crusher that was cleaned extensively with deionized water before each course, and milled in an agate mortar in order to minimize the potential contamination of transitional metals. 5 g of each sample pulp was pulverized to 100-mesh size and then about 1 g was dried at 110 °C and heated to 1000 °C for 3 h for chemical preparation. A 200 mg fraction of each sample was then mixed with 900 mg lithium tetraborate in a vitreous graphite crucible and fused at 1000 °C in a silica muffle furnace under an atmospheric pressure of argon for 30 min. After cooling, the obtained glass was directly dissolved in the crucible containing dilute 100 mL of 4% $HNO_3$ and glycerine. This solution was then analyzed by inductively coupled plasma – mass spectrometry. Detection limits were 5 ppm for Cu, Ni, Zn, V and Pb; 2 ppm for Zr, Mo; 1 ppm for Ag, W, Sn; 0.5 ppm for La, Ba, Ce, Co, Y, Tl; 0.2 ppm for Nb, Rb; 0.1 ppm for Nd, Ga, Sr, Ta; 0.05 ppm for U, Th, Gd; 0.03 ppm for Er, Eu, Yb, Pr, Sm; 0.01 ppm for Ho, Cs, Lu, Tb, Tm; 0.2 ppm for Hf; 10 ppm for Cr. For XRF analysis, 900 mg of each sample was added to 9 g of lithium

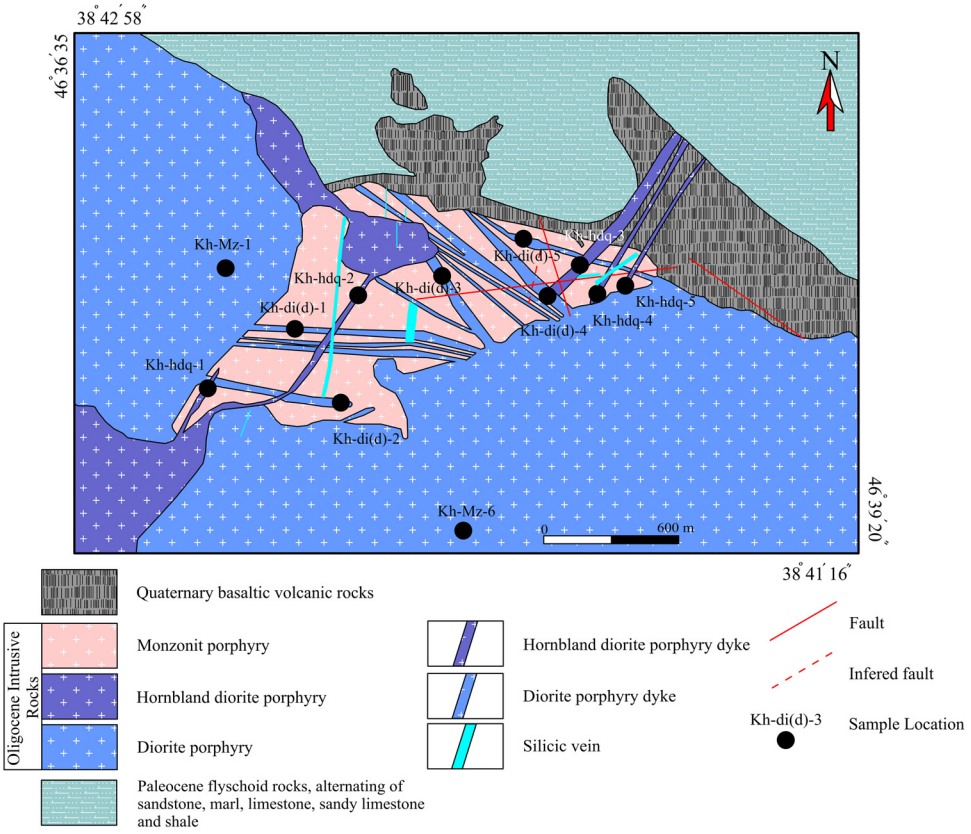


**Fig. 2.** Detailed geological map of the Khoynarood area, showing the distribution of intrusive bodies and dikes. The location of the studied samples are also shown.

borate flux (50%–50% $Li_2Br_4O_7$–$LiBO_2$), mixed well and fused in an auto fluxer between 1050–1100 °C. A flat molten glass disc was prepared from the resulting melt. Then the disc was analyzed by X-ray fluorescence spectrometry. Detection limits for all oxides were about 0.01 wt%.

## 4. Results and discussion

### 4.1. Petrography of the intrusive rocks and related dikes

#### 4.1.1. Quartz-monzodiorite

The main rock-forming minerals of this intrusive body are plagioclase (with polysynthetic twining and oscillatory concentric zoning; 30–40%), amphibole (5–10%), K-feldspar (20–25%), quartz (10–15%) and subordinate amounts of biotite (0–5%), portraying a porphyritic texture with a fine- to medium-grained groundmass (Fig. 3a). The accessory minerals are zircon, apatite and titanite. Weak to moderate propylitic (partial replacement of plagioclase and amphibole crystals by epidote; Fig. 3b) and weak to intense phyllic alterations, as well as different combinations of these assemblages are visible in this body.

#### 4.1.2. Diorite

This intrusive unit displays fine- to medium-grained porphyritic, as well as microlitic porphyritic and ophitic textures (Fig. 3c and d). Plagioclase and amphibole phenocrysts are recognizable in hand specimens. Hyalomicrolitic porphyritic texture is also found in some samples, which may be related to the rapidly cooled margins of this body.

The main minerals are plagioclase (50–60%) and amphibole (10–20%), along with quartz (0–5%), K-feldspar (0–10%) and lesser biotite, with accessory amounts of apatite, pyrite and magnetite (Fig. 3c and d). Plagioclase is found as both phenocrysts and fine microlites within the groundmass. It is locally epidotized and displays concentric zoning (Fig. 3d). Amphibole crystals are often euhedral and in some parts, appear as fine grains within the groundmass (Fig. 3c). Quartz occurs interstitially between other crystals. Biotites are often altered to muscovite–chlorite or epidote–chlorite assemblages. Spherulitic aggregates of chlorite are locally found in the groundmass as a result of propylitic alteration.

#### 4.1.3. Hornblende-diorite

The alteration degree of this intrusive body is less than the porphyritic diorite stock, so that the characteristic feature of this stock is the co-existence of fresh amphibole and biotite. Moreover, its coarse amphibole crystals are visible in hand specimen. It shows porphyritic texture with fine-grained, coarse-grained and microlitic groundmass (Fig. 3e and f). The main minerals are plagioclase with oscillatory concentric zoning (40–50%) and euhedral amphibole (20–30%) with subordinate amounts of biotite (0–10%), quartz (0–5%) and K–feldspar (0–5%); the latter two mineral are found as fine grains within the groundmass. Accessory minerals are apatite and magnetite.

#### 4.1.4. Granodiorite

This intrusive unit is comprised of plagioclase (30–40%), K-feldspar (25–35%) and quartz (10–15%) (Fig. 3g and h). K-feldspar and quartz are anhedral, while plagioclase crystals are subhedral with slight sericitic and argillic alteration. Biotite is a subordinate mineral, showing alteration to Fe-oxides. The main textures observed in this stock are granular, granophyric and mortar (Fig. 3g and h); the latter, along with oscillatory extinction of quartz grains, is formed due to the deformation. Microlitic porphyritic texture is also locally found, with plagioclase, amphibole and biotite phenocrysts set in a fine-grained groundmass, testifying to the shallow depth of emplacement and its rapid cooling.

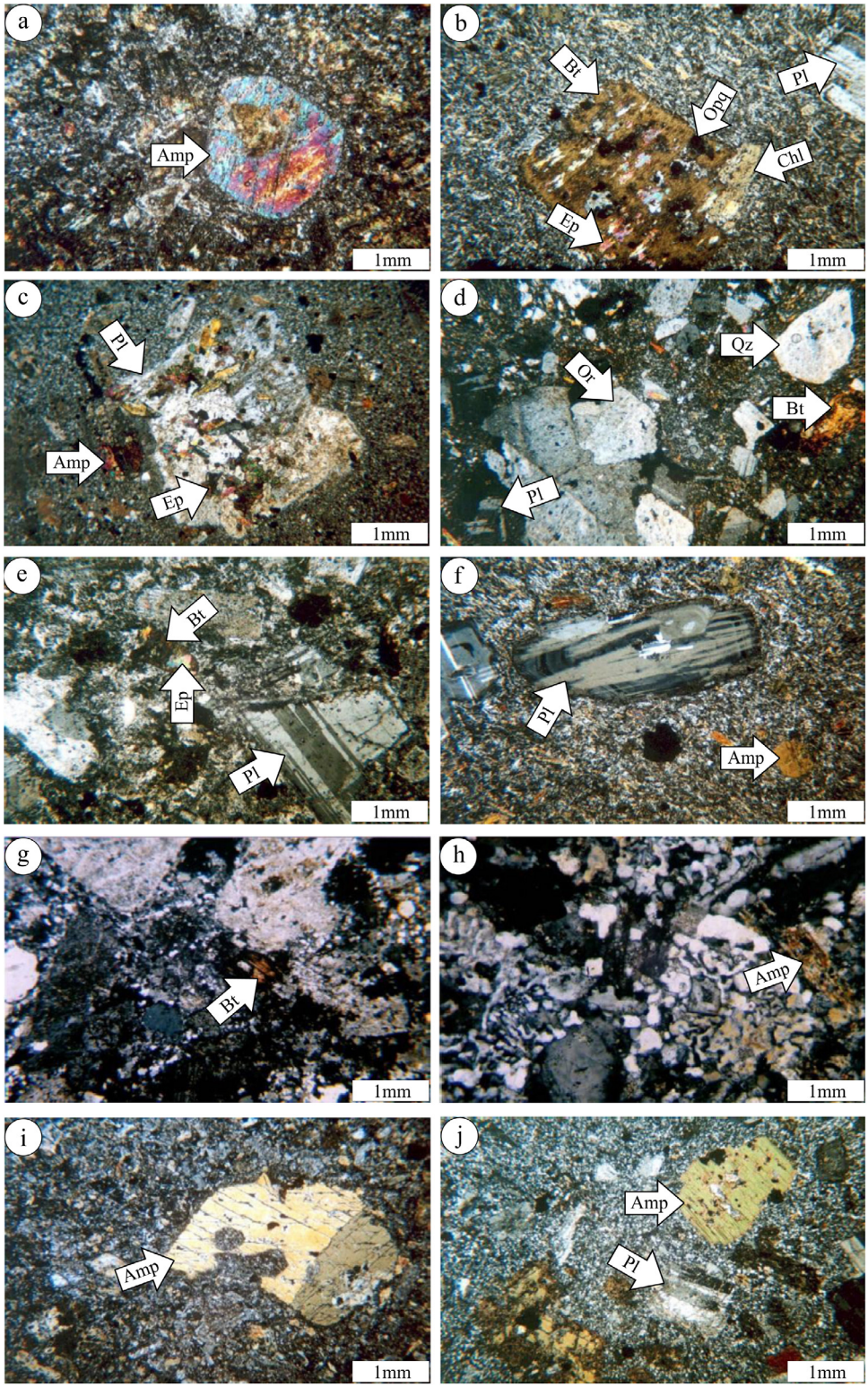


**Fig. 3.** Photomicrographs of the intrusive rocks in Khoynarood. (a) Fine-grained porphyritic texture along with moderate propylitic alteration and a euhedral amphibole phenocryst within the diorite porphyry body. (b) Porphyritic texture with fine-grained groundmass and weak to moderate propylitic alteration within the diorite porphyry body. (c) Epidotization of a plagioclase and an amphibole phenocryst within monzonite–quartz monzonite body. (d) Porphyritic texture with fine- to medium-grained groundmass and weak phyllic–moderate propylitic alteration within monzonite–quartz monzonite body. (e) Porphyritic texture with coarse-grained groundmass and moderate propylitic–weak argillic alteration in hornblende-diorite porphyry body. (f) Microlitic porphyritic texture and weak propylitic alteration, along with zoned plagioclase phenocrysts within hornblende-diorite porphyry body. (g) Granular and mortar textures and the marginal alteration of biotite to Fe-oxide within granodiorite body. (h) Granophyric texture within the granodiorite body. (i) Microlitic porphyritic texture and weak propylitic alteration within porphyritic dioritic dikes. (j) Porphyritic texture with fine-grained groundmass and weak propylitic alteration within hornblende-dioritic porphyritic dikes. Mineral abbreviations from Whitney and Evans (2010).

#### 4.1.5. Dioritic dikes

These dikes share the compositional and textural features of the porphyritic diorite stock and cross-cut the porphyritic monzonite stock with the major trend of NW–SE. The main minerals are plagioclase (45–55%) and amphibole (10–20%), with lesser amounts of quartz (0–5%), K-feldspar (5–10%) and biotite (0–5%) (Fig. 3i). Accessory minerals are pyrite, magnetite and apatite. The main textures observed in these dikes are hyalomicrolitic porphyritic and microlitic porphyritic and they display weak phyllic and weak to moderate propylitic alterations (Fig. 3i).

#### 4.1.6. Hornblende-dioritic dikes

They are composed of fresh, euhedral to subhedral amphibole (20–35%), plagioclase with oscillatory concentric zoning (40–50%), and lesser amounts of mostly fresh biotite phenocrysts (0–10%) (Fig. 3j). Quartz (0–5%) is found within the groundmass along with accessory minerals of apatite, pyrite and magnetite. They display hyaloporphyritic to hyalomicrolitic porphyritic and microlitic porphyritic textures (Fig. 3j).

### 4.2. Geochemistry of the studied intrusions and related dikes

In order to study the geochemistry of the Khoynarood intrusive bodies and the related dikes, fresh samples of monzonite, granodiorite, porphyritic diorite–quartz diorite bodies, as well as diorite–quartz diorite and hornblende-diorite dikes were analyzed (Table 1). The data were used for geochemical and petrogenetic classifications and discussions, except the samples No. gd4, ddi1 and dhdi1, for which the total oxide content was below 97%. According to the TAS diagram of Cox et al. (1979), all of the intrusive samples are classified as monzonite and diorite, and as the diorite and hornblende-diorite dike samples plot within the monzonite filed, while those of the granodioritic intrusion fall within the granodiorite field (Fig. 4a). Based on the $K_2O$–$SiO_2$ diagram (Rickwood, 1989), all the samples plot within the moderate- to high-K calk alkaline field (Fig. 4b). In tectonic setting discrimination diagrams, the data points are plotted in the active continental margin volcanic arc field (Pearce et al., 1984; Fig. 5), lying within the post-collisional area proposed by Pearce (1996; Fig. 5b). The high $SiO_2$ (58.3–68.1%), $Al_2O_3$ (14.1–18.6%), MgO (0.7–4.3%), $K_2O/Na_2O$ (0.26–0.58), $Fe_2O_3 + MnO + MgO + TiO_2$ (4.27–13.13%) values and the low Y (8–17 ppm) and HREE (e.g., Yb about 1–2 ppm) contents, the high Sr concentration (750–1330 ppm) and high Ba/La (13.51–50.96), $(La/Yb)_N$ (7–22), Sr/Y (57.6–166.2), Rb/La (1.1–3) and La/Yb (10–33.63) ratios correspond to the geochemical characteristics of adakites (Moyen, 2009) and testify to the adakitic nature of the studied intrusive bodies and the related dikes. Based on the diagrams provided by Martin et al. (2005) to discriminate adakites from arc magmas of the classic subduction zones (Fig. 6a and b), the studied samples lie within the adakite field. The high Sr/Y ratio (60.53–166.25) reflects the high depth of melting and incorporation of plagioclase in the melting process, as plagioclase becomes unstable by pressure increase and consequently, Sr is released. On the other hand, remaining of garnet as a residual phase in the source area or garnet differentiation from magma at deep levels can be responsible for the low Y content and high Sr/Y ratio (Moyen, 2009). Additionally, based on the plotted data points in the discriminating diagrams for LSA and HSA (Martin et al., 2005; Fig. 6c–e), it can be seen that the studied rocks are of HSA type, which are typically originated from melting of the subducting oceanic slab in the garnet-stability field. Furthermore, LSAs have more differentiated REE pattern compared to HSAs (showing concave HREE pattern) and are, is characterized by higher Sr/Y and La/Yb ratios (the latter about 10 in LSA). On this basis, the Sr/Y and La/Yb ratios and the REE pattern of the studied rocks (60.5–166.2 and 10–33.63, respectively) do not correspond to low-silica adakites.

Richards and Kerrich (2007) argue that major part of the differentiated calc-alkaline magmas show false adakitic characteristics, owing to the differentiation of amphibole and garnet and a decrease in Y and HREE. However, the Sr/Y ratio in the studied rocks is higher than the La/Yb ratio and so, according to Richards and Kerrich (2007), they can be considered as real adakites. Moreover, Richards and Kerrich (2007) believe that adakitic signatures such as low Y and Yb contents and high Sr/Y and La/Yb ratios can also be related to the processes such as partial melting or fractional crystallization. According to La/Yb vs. La plot in Fig. 7a, the compositional trend of the studied bodies corresponds well to the partial melting, rather than fractional crystallization. Furthermore, the data point trend in the Ba/Nb vs. Nb plot (Fig. 7b) also testifies to the occurrence of partial melting (Bourdon et al., 2002).

Therefore, the intrusive rocks in the Khoynarood share essential similarities with HSAs, as their $SiO_2$ content is generally higher than 58%, the distribution pattern of the HREEs is concave (Fig. 8) and their Yb/Lu ratio is between 5.6 and 15.7, they have similar range of MgO and $SiO_2$ compared to the high-silica (Martin et al., 2005) and low-Mg (Danyushevsky et al., 2008) adakites. On the other hand, the K/Na ratio (0.03–0.6) in the Khoynarood bodies is very low, and their $K_2O$ content is in the same range of the other reported high-silica adakites (e.g., Jahangiri, 2007; Eyuboglu et al., 2011a,b; Eyuboglu et al., 2012; Eyuboglu et al., 2013; Simmonds, 2013). This fact clearly distinguishes them from C-type adakites, which have K/Na ratios varying between 0.7 and 2 (Table 1).

Primitive mantle- (Sun and McDonough, 1989) and chondrite-normalized (McDonough and Sun, 1995) distribution patterns of the rare earth elements for the studied rocks testify to the genetic relationship among these intrusive bodies and their cross-cutting dikes, displaying enrichments of LREEs and LILEs and depletions of HREEs and HFSEs (Fig. 8). Such a pattern is characteristic of arc magmatism in the subduction zones (Nicholson et al., 2004) and can be found in any magma sourced from a subducted oceanic crust and the overlying metasomatized mantle wedge, which has undergone partial crystallization, assimilation and contamination with crustal materials, while HREEs and HFSEs have remained in the source rock (e.g., Sheth et al., 2002).

LREE enrichment can be attributed to the low-degree partial melting and/or magma contamination by crustal materials (Almeida et al., 2007). Based on the chondrite-normalized spider diagrams, the studied bodies do not show negative Eu anomaly, rejecting the remaining of plagioclase as a residual phase within the source materials or its differentiation during crystallization (Arslan and Aslan, 2006). Moreover, the high Sr content signifies the lack of residual or differentiated plagioclase. Contrarily, residuals of minerals like hornblende, titanite and zircon lead to positive Eu anomaly (Rollinson, 1993). The low HREE and Y contents may be due to the presence of garnet and/or amphibole in the source rock residue. It was shown that fractional crystallization of the magma has not occurred during the evolution of the studied rocks. Moreover, the remaining of amphibole within the source rock residue is also supported by the spoon-like distribution pattern of REEs in Fig. 8.

The negative anomalies of HFSE (e.g., Nb, Ta and Ti; Fig. 8) are characteristic of arc environments, though it may also be resulted from magma contamination with crustal materials during its ascending and emplacement above the Benioff zone. However, many researchers relate the depletion of these elements in the metasomatizing fluids of the mantle wedge to the presence of HFSE-bearing residual high-temperature phases (e.g., rutile, ilmenite, Ti-bearing pargasitic amphibole, titanite and apatite) in the eclogitic rocks of the subducting oceanic crust or in the mantle wedge of the source area (Martin, 1999). Some researchers believe that Cl-rich fluids are responsible for the depletion of HFSEs and enrichment of LILEs in arc magmas (Keppler, 1996). Additionally,

**Table 1**
XRF and ICP-MS analysis data of the studied intrusive rocks and dikes in Khoynarood. Oxides are given in wt% and trace elements in ppm (Mz: monzonite, gd: granodiorite, di: diorite, ddi: dioritic dikes, dhdi: hornblend-dioritic dikes).

| Major Oxides (wt%) | Mz1 | Mz2 | Mz3 | Mz4 | Mz5 | Mz6 | Mz7 | Mz8 | Mz9 | Mz10 | gd1 | gd2 | gd3 | gd4 | gd5 |
|---|---|---|---|---|---|---|---|---|---|---|---|---|---|---|---|
| $SiO_2$ | 59.50 | 60.59 | 58.44 | 58.96 | 61.30 | 61.55 | 58.32 | 58.80 | 63.54 | 60.35 | 64.01 | 64.41 | 66.19 | 63.54 | 68.12 |
| $TiO_2$ | 0.85 | 0.79 | 0.98 | 1 | 0.64 | 0.78 | 0.84 | 1.35 | 0.83 | 0.74 | 0.48 | 0.42 | 0.43 | 0.46 | 0.44 |
| $Al_2O_3$ | 15.71 | 14.13 | 15.46 | 16.54 | 18.15 | 16.43 | 16.67 | 17.83 | 17.54 | 18.65 | 17.89 | 16.85 | 16.77 | 17.14 | 17.07 |
| $Fe_2O_3$ | 6.58 | 6.71 | 7.74 | 6.84 | 5.02 | 5.97 | 6.32 | 7.52 | 5.98 | 5.78 | 7.38 | 3.18 | 4.53 | 3.84 | 3.89 |
| MnO | 0.07 | 0.08 | 0.14 | 0.07 | 0.01 | 0.01 | 0.07 | 0.13 | 0.06 | 0.06 | 0.06 | 0.04 | 0.01 | 0.05 | 0.01 |
| MgO | 2.32 | 3.80 | 4.27 | 2.91 | 1.29 | 0.85 | 2.23 | 1.62 | 0.98 | 0.68 | 0.93 | 1.73 | 0.77 | 1.22 | 0.95 |
| CaO | 6.92 | 4.31 | 4.98 | 6.95 | 6.75 | 5.65 | 6.45 | 5.78 | 5.63 | 5.82 | 2.71 | 3.38 | 3.19 | 2.78 | 2.35 |
| $Na_2O$ | 6.15 | 5.91 | 5.70 | 5.72 | 4.94 | 5.80 | 4.87 | 4.78 | 5.95 | 5.89 | 5.35 | 5.04 | 4.11 | 4.82 | 4.22 |
| $K_2O$ | 1.61 | 1.67 | 1.95 | 1.69 | 2.66 | 2.71 | 1.52 | 1.79 | 2.35 | 2.98 | 2.41 | 2.95 | 2.32 | 2.06 | 1.89 |
| $P_2O_5$ | 0.52 | 0.20 | 0.48 | 0.46 | 0.19 | 0.15 | 0.50 | 0.46 | 0.14 | 0.13 | 0.14 | 0.12 | 0.28 | 0.17 | 0.17 |
| Total | 100.23 | 98.19 | 100.14 | 101.14 | 100.95 | 99.90 | 97.79 | 100.06 | 102.91 | 101.08 | 101.36 | 98.13 | 98.61 | 96.08 | 99.10 |
| Mg# | 0.35 | 0.46 | 0.46 | 0.39 | 0.28 | 0.18 | 0.35 | 0.25 | 0.20 | 0.15 | 0.16 | 0.45 | 0.20 | 0.33 | 0.27 |
| Elements (ppm) | | | | | | | | | | | | | | | |
| Ba | 604 | 846 | 924 | 662 | 764 | 836 | 698 | 840 | 1427 | 1325 | 717 | 543 | 633 | 1044 | 789 |
| Rb | 67 | 33 | 75 | 76 | 48 | 42 | 52 | 82 | 74 | 69 | 51 | 48 | 63 | 68 | 67 |
| Sr | 1330 | 924 | 988 | 1311 | 884 | 827 | 1292 | 750 | 981 | 787 | 1108 | 1154 | 1122 | 907 | 1173 |
| Zr | 134 | 121 | 125 | 151 | 137 | 121 | 128 | 114 | 139 | 128 | 105 | 136 | 108 | 131 | 117 |
| Nb | 18 | 11 | 12 | 20 | 16 | 12 | 11 | 17 | 16 | 15 | 10 | 15 | 17 | 12 | 11 |
| Ni | 22 | 28 | 24 | 22 | 42 | 33 | 20 | 29 | 24 | 30 | 47 | 35 | 39 | 33 | 30 |
| Co | 17 | 13 | 14 | 16 | 13 | 14 | 15 | 16 | 14 | 13 | 12 | 15 | 12 | 10 | 16 |
| Zn | 78 | 53 | 62 | 79 | 86 | 92 | 69 | 75 | 72 | 89 | 88 | 62 | 75 | 50 | 58 |
| Cr | 79 | 83 | 61 | 86 | 82 | 42 | 69 | 48 | 57 | 90 | 65 | 63 | 81 | 46 | 72 |
| Y | 8 | 11 | 10 | 11 | 8 | 10 | 11 | 12 | 10 | 13 | 12 | 8 | 9 | 12 | 12 |
| Cs | 1 | 1.9 | 2.2 | 1.5 | 2.5 | 2 | 1.9 | 1.7 | 2.2 | 2.5 | 1.5 | 2 | 2.2 | 1.8 | 1.3 |
| Ta | 0.8 | 0.9 | 1 | 0.9 | 1.1 | 0.8 | 0.7 | 0.7 | 1 | 1.1 | 0.9 | 0.7 | 1 | 1.1 | 0.7 |
| Hf | 5 | 4 | 4 | 3 | 5 | 6 | 5 | 3 | 3 | 4 | 4 | 4 | 3 | 4 | 5 |
| Cu | 14 | 8 | 8 | 11 | 16 | 38 | 13 | 7 | 16 | 20 | 38 | 46 | 16 | 5 | 32 |
| Ga | 18 | 22 | 21 | 18 | 16 | 25 | 28 | 21 | 17 | 19 | 20 | 19 | 15 | 25 | 24 |
| Pb | 19 | 12 | 16 | 11 | 12 | 13 | 16 | 14 | 17 | 15 | 15 | 18 | 12 | 14 | 12 |
| Th | 12 | 15 | 11 | 16 | 14 | 14 | 12 | 11 | 13 | 12 | 14 | 17 | 15 | 15 | 12 |
| U | 5 | 3 | 5 | 4 | 7 | 6 | 6 | 4 | 3 | 5 | 4 | 3 | 9 | 3 | 5 |
| V | 110 | 87 | 98 | 81 | 76 | 64 | 119 | 95 | 92 | 98 | 90 | 67 | 69 | 80 | 74 |
| W | 1 | 1 | 1 | 1 | 6 | 1 | 1 | 2 | 1 | 1 | 1 | 5 | 1 | 2 | 1 |
| La | 40 | 29 | 45 | 49 | 26 | 22 | 38 | 40 | 37 | 26 | 36 | 40 | 40 | 27 | 26 |
| Ce | 68 | 40 | 66 | 62 | 67 | 70 | 65 | 59 | 50 | 44 | 55 | 58 | 46 | 41 | 65 |
| Pr | 4.4 | 4.8 | 8.2 | 8.7 | 8.9 | 5.3 | 7.2 | 8.8 | 8.4 | 5.1 | 5.3 | 4.9 | 6.6 | 6.7 | 7.4 |
| Nd | 17 | 18 | 17 | 18 | 20 | 19 | 18 | 21 | 17 | 16 | 17 | 21 | 21 | 16 | 16 |
| Sm | 2.7 | 2.6 | 4.5 | 2.9 | 3.5 | 4.5 | 5.1 | 3.9 | 4.1 | 2.5 | 2.5 | 2.6 | 3.4 | 4.2 | 4.3 |
| Eu | 0.7 | 0.9 | 1.4 | 0.8 | 1 | 1.2 | 0.8 | 0.8 | 0.9 | 1.1 | 0.8 | 1.6 | 1.7 | 1.2 | 0.8 |
| Gd | 2 | 2.3 | 2.9 | 2.45 | 2.7 | 3.8 | 3.9 | 4 | 2.5 | 1.9 | 2.1 | 2.5 | 2.1 | 3.4 | 3.5 |
| Tb | 0.4 | 0.3 | 0.7 | 0.6 | 0.3 | 0.2 | 0.4 | 0.3 | 0.6 | 0.7 | 0.4 | 0.5 | 0.7 | 0.5 | 0.4 |
| Dy | 2.2 | 2.4 | 2.6 | 1.8 | 2.1 | 2.4 | 2.8 | 2.7 | 2 | 1.8 | 2.3 | 1.9 | 2.1 | 2 | 1.9 |
| Er | 0.9 | 1.1 | 1.2 | 0.8 | 1.4 | 1.2 | 1.3 | 0.9 | 1.1 | 1.6 | 1.2 | 0.9 | 1.5 | 1 | 1.5 |
| Tm | 0.17 | 0.25 | 0.2 | 0.18 | 0.26 | 0.21 | 0.19 | 0.15 | 0.17 | 0.2 | 0.19 | 0.17 | 0.24 | 0.24 | 0.2 |
| Yb | 2 | 1.3 | 2.2 | 1.8 | 2 | 2 | 1.9 | 1.4 | 1.1 | 1.7 | 2.1 | 1.6 | 2.2 | 1.5 | 2.1 |
| Lu | 0.24 | 0.15 | 0.14 | 0.15 | 0.19 | 0.15 | 0.17 | 0.18 | 0.16 | 0.17 | 0.2 | 0.2 | 0.17 | 0.13 | 0.16 |
| Sr/Y | 166.25 | 84 | 98.8 | 119.18 | 110.5 | 82.7 | 117.45 | 62.5 | 98.1 | 60.54 | 92.33 | 144.25 | 124.66 | 75.58 | 97.75 |
| La/Yb N | 13.33 | 14.87 | 13.63 | 18.14 | 8.66 | 7.33 | 13.33 | 19.04 | 22.42 | 10.19 | 11.42 | 16.66 | 12.12 | 12 | 8.25 |
| Yb N | 7.97 | 3.61 | 3.44 | 5.01 | 4.49 | 3.65 | 2.99 | 3.55 | 2.86 | 4.13 | 5.16 | 5.23 | 3.17 | 2.26 | 3.54 |

| Major Oxides (wt%) | gd6 | gd7 | gd8 | di1 | di2 | di3 | dhdi1 | dhdi2 | dhdi3 | dhdi4 | ddi1 | ddi2 | ddi3 | ddi4 | ddi5 |
|---|---|---|---|---|---|---|---|---|---|---|---|---|---|---|---|
| $SiO_2$ | 65.15 | 67.35 | 63.94 | 63.40 | 64.10 | 63.78 | 61.80 | 62.15 | 62.92 | 61.90 | 60.95 | 60.47 | 61.09 | 60.84 | 59.92 |
| $TiO_2$ | 0.47 | 0.43 | 0.49 | 0.75 | 0.68 | 0.80 | 0.70 | 0.65 | 0.84 | 0.69 | 0.62 | 0.74 | 0.78 | 0.67 | 0.71 |
| $Al_2O_3$ | 16.67 | 16.94 | 17.27 | 16.70 | 17.10 | 16.95 | 15.90 | 16.24 | 16.41 | 16.02 | 16.10 | 16.45 | 16.28 | 15.98 | 16.76 |
| $Fe_2O_3$ | 6.57 | 4.57 | 4.21 | 4.33 | 5.14 | 4.90 | 4.70 | 5.27 | 5.37 | 4.94 | 4.70 | 4.23 | 4.61 | 4.54 | 4.20 |
| MnO | 0.07 | 0.01 | 0.09 | 0.04 | 0.07 | 0.07 | 0.08 | 0.06 | 0.04 | 0.09 | 0.07 | 0.07 | 0.09 | 0.08 | 0.07 |
| MgO | 0.84 | 0.81 | 1.52 | 1.90 | 1.85 | 2.14 | 1.89 | 2.05 | 2.18 | 1.90 | 1.97 | 2.14 | 1.95 | 2.06 | 1.93 |
| CaO | 2.89 | 2.26 | 3.14 | 3.74 | 4.70 | 4.82 | 3.94 | 4.28 | 4.11 | 3.81 | 4.09 | 3.72 | 4.10 | 4.54 | 4.26 |
| $Na_2O$ | 4.67 | 4.57 | 5.28 | 5.41 | 4.95 | 5.10 | 4.98 | 5.02 | 5.10 | 4.90 | 5.46 | 5.70 | 5.81 | 5.62 | 5.77 |
| $K_2O$ | 2.14 | 2.07 | 2.61 | 2.34 | 2.10 | 2.74 | 2.15 | 2.35 | 2.33 | 2.28 | 2.47 | 2.98 | 2.93 | 2.66 | 2.81 |
| $P_2O_5$ | 0.19 | 0.18 | 0.15 | 0.20 | 0.42 | 0.30 | 0.24 | 0.41 | 0.42 | 0.49 | 0.39 | 0.57 | 0.50 | 0.51 | 0.57 |
| Total | 99.96 | 99.19 | 98.70 | 98.81 | 101.11 | 101.60 | 96.38 | 98.48 | 99.72 | 97.02 | 96.82 | 97.07 | 98.11 | 97.50 | 97.02 |
| Mg# | 0.16 | 0.21 | 0.36 | 0.40 | 0.35 | 0.40 | 0.38 | 0.37 | 0.38 | 0.37 | 0.39 | 0.44 | 0.39 | 0.41 | 0.41 |
| Elements (ppm) | | | | | | | | | | | | | | | |
| Ba | 671 | 975 | 992 | 990 | 1050 | 984 | 1045 | 1029 | 1058 | 991 | 998 | 1017 | 1081 | 1026 | 986 |
| Rb | 54 | 59 | 74 | 45 | 52 | 50 | 49 | 52 | 68 | 56 | 61 | 58 | 66 | 52 | 64 |
| Sr | 1069 | 948 | 1087 | 890 | 920 | 1015 | 880 | 945 | 957 | 921 | 1105 | 1095 | 1251 | 1214 | 1081 |
| Zr | 121 | 126 | 141 | 125 | 131 | 127 | 125 | 137 | 148 | 114 | 142 | 150 | 152 | 147 | 159 |
| Nb | 16 | 14 | 14 | 11 | 17 | 21 | 18 | 18 | 16 | 17 | 20 | 23 | 19 | 21 | 20 |
| Ni | 54 | 38 | 39 | 27 | 24 | 30 | 45 | 38 | 49 | 47 | 36 | 41 | 37 | 44 | 40 |
| Co | 18 | 12 | 19 | 14 | 17 | 20 | 20 | 18 | 26 | 31 | 17 | 21 | 20 | 25 | 18 |
| Zn | 73 | 67 | 51 | 49 | 78 | 56 | 39 | 46 | 54 | 51 | 52 | 50 | 56 | 49 | 54 |

Table 1 (*Continued*)

| Major Oxides (wt%) | gd6 | gd7 | gd8 | di1 | di2 | di3 | dhdi1 | dhdi2 | dhdi3 | dhdi4 | ddi1 | ddi2 | ddi3 | ddi4 | ddi5 |
|---|---|---|---|---|---|---|---|---|---|---|---|---|---|---|---|
| Cr | 85 | 59 | 63 | 68 | 85 | 59 | 86 | 91 | 96 | 112 | 78 | 73 | 81 | 76 | 74 |
| Y | 16 | 14 | 17 | 12 | 12 | 12 | 12 | 13 | 11 | 16 | 10 | 11 | 13 | 17 | 12 |
| Cs | 3.3 | 2.1 | 2.2 | 2.4 | 2.1 | 1.9 | 2.4 | 2 | 3.6 | 1.9 | 1.9 | 1.6 | 2.9 | 1.6 | 3.4 |
| Ta | 1.2 | 0.9 | 0.7 | 0.9 | 1.1 | 0.8 | 0.8 | 1.1 | 0.7 | 1.3 | 0.8 | 1 | 1.2 | 0.7 | 0.9 |
| Hf | 5 | 4 | 6 | 3 | 5 | 3 | 6 | 6 | 8.5 | 7 | 4 | 3 | 5 | 4 | 6 |
| Cu | 42 | 39 | 14 | 36 | 25 | 40 | – | – | – | – | – | – | – | – | – |
| Ga | 24 | 27 | 22 | 18 | 22 | 24 | 20 | 21 | 17 | 24 | 19 | 17 | 21 | 20 | 25 |
| Pb | 24 | 19 | 14 | 14 | 14 | 18 | 14 | 17 | 21 | 16 | 18 | 11 | 19 | 22 | 15 |
| Th | 16 | 18 | 17 | 16 | 14 | 16 | 18 | 17 | 22 | 25 | 17 | 15 | 21 | 18 | 19 |
| U | 7 | 8 | 12 | 6 | 7 | 5 | 4 | 4 | 7 | 5 | 5 | 5 | 6 | 5 | 7 |
| V | 79 | 78 | 83 | 76 | 84 | 81 | 90 | 94 | 98 | 87 | 85 | 74 | 78 | 87 | 76 |
| W | 5 | 3 | 2 | 2 | 4 | 1 | 2 | 2 | 5 | 3 | 3 | 5 | 4 | 3 | 4 |
| La | 39 | 31 | 25 | 24 | 21 | 24 | 36 | 32 | 35 | 31 | 41 | 38 | 40 | 40 | 37 |
| Ce | 54 | 45 | 47 | 62 | 59 | 61 | 57 | 54 | 61 | 55 | 61 | 63 | 66 | 59 | 61 |
| Pr | 5.1 | 6.4 | 7.1 | 6.8 | 7.4 | 7.2 | 7.2 | 7.2 | 8.1 | 7.5 | 7.7 | 8.1 | 10 | 9 | 12.4 |
| Nd | 19 | 18 | 20 | 18 | 17 | 20 | 21 | 21 | 20 | 24 | 20 | 18 | 21 | 19 | 20 |
| Sm | 3.7 | 3.9 | 3.9 | 3.1 | 3.7 | 2.9 | 3.4 | 3.1 | 3.2 | 3.6 | 2.9 | 2.7 | 3.6 | 3.1 | 3.8 |
| Eu | 1.1 | 1.1 | 1.2 | 1.1 | 0.9 | 0.8 | 1.1 | 0.9 | 1.25 | 1.6 | 0.7 | 0.6 | 0.8 | 0.75 | 0.68 |
| Gd | 2.7 | 3.4 | 3.7 | 1.8 | 2.8 | 2.4 | 2.7 | 2.8 | 3.3 | 3.3 | 2.6 | 2.1 | 1.9 | 2.6 | 3.4 |
| Tb | 0.65 | 0.6 | 0.62 | 0.6 | 0.5 | 0.6 | 0.5 | 0.5 | 0.5 | 0.7 | 0.5 | 0.7 | 0.6 | 0.4 | 1.1 |
| Dy | 2.2 | 2.16 | 2.26 | 2.4 | 1.8 | 1.9 | 2.2 | 2.4 | 2.1 | 2.5 | 2.3 | 1.9 | 1.8 | 2.5 | 2.6 |
| Er | 1.2 | 0.9 | 0.9 | 1.2 | 0.9 | 1.5 | 0.9 | 1.1 | 1 | 1.1 | 1.4 | 1.5 | 1.2 | 1.6 | 1.8 |
| Tm | 0.19 | 0.22 | 0.25 | 0.22 | 0.21 | 0.19 | 0.18 | 0.18 | 0.25 | 0.19 | 0.22 | 0.21 | 0.32 | 0.2 | 0.59 |
| Yb | 1.8 | 1.7 | 1.9 | 1.8 | 2.1 | 1.7 | 1.6 | 1.8 | 1.8 | 2.3 | 1.8 | 2 | 2.4 | 1.9 | 2.1 |
| Lu | 0.26 | 0.17 | 0.21 | 0.15 | 0.16 | 0.2 | 0.28 | 0.24 | 0.32 | 0.23 | 0.22 | 0.19 | 0.25 | 0.18 | 0.36 |
| Sr/Y | 66.81 | 67.71 | 63.94 | 74.16 | 76.66 | 92.27 | 73.33 | 72.69 | 87 | 57.56 | 110.5 | 99.54 | 96.23 | 71.41 | 90.08 |
| La/Yb N | 15.54 | 13.08 | 9.44 | 8.88 | 6.66 | 9.41 | 15 | 11.85 | 13.95 | 9.67 | 15.18 | 12.66 | 11.96 | 15.10 | 12.64 |
| Yb N | 3.65 | 3.44 | 3.85 | 4.69 | 3.74 | 4.93 | 3.93 | 4.08 | 3.65 | 4.66 | 4.93 | 5.47 | 3.37 | 2.43 | 4.86 |

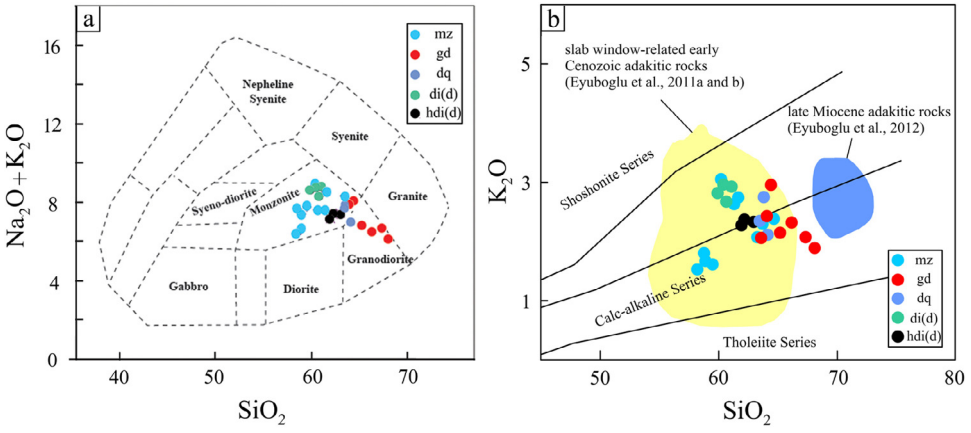


**Fig. 4.** (a) TAS igneous rock classification diagram (Cox et al., 1979) and (b) $K_2O$ vs. $Na_2O$ diagram (Rickwood, 1989) to discriminate magma series, and the plotted data points of the analyzed samples (sample symbols as Table 1).

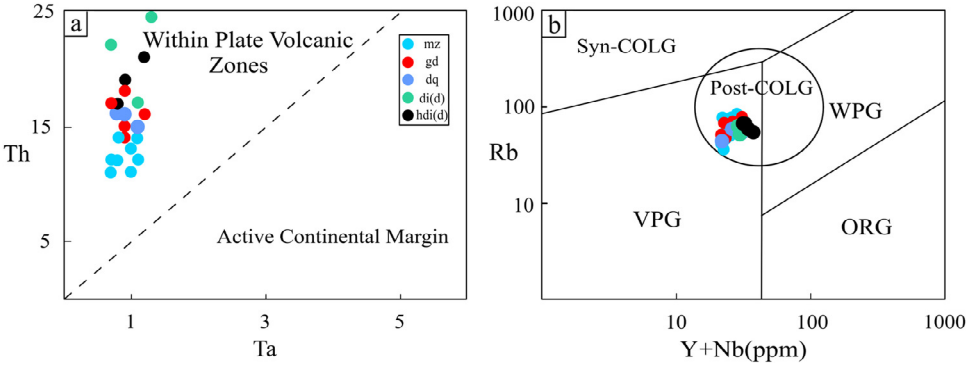


**Fig. 5.** (a) Th–Ta (Schandl and Gorton, 2002) and (b) Rb versus (Y–Nb) (Pearce et al., 1984) diagrams to distinguish the tectonic setting of the magmatic rocks; the area presenting the post-collisional setting is from Pearce (1996) (sample symbols as Table 1).

the solubility of these elements in water plays a great role in their distribution within the arc magmas, as LILEs are soluble and can easily be leached by the metasomatizing fluids released from the subducted oceanic slab and carried into the source region of arc

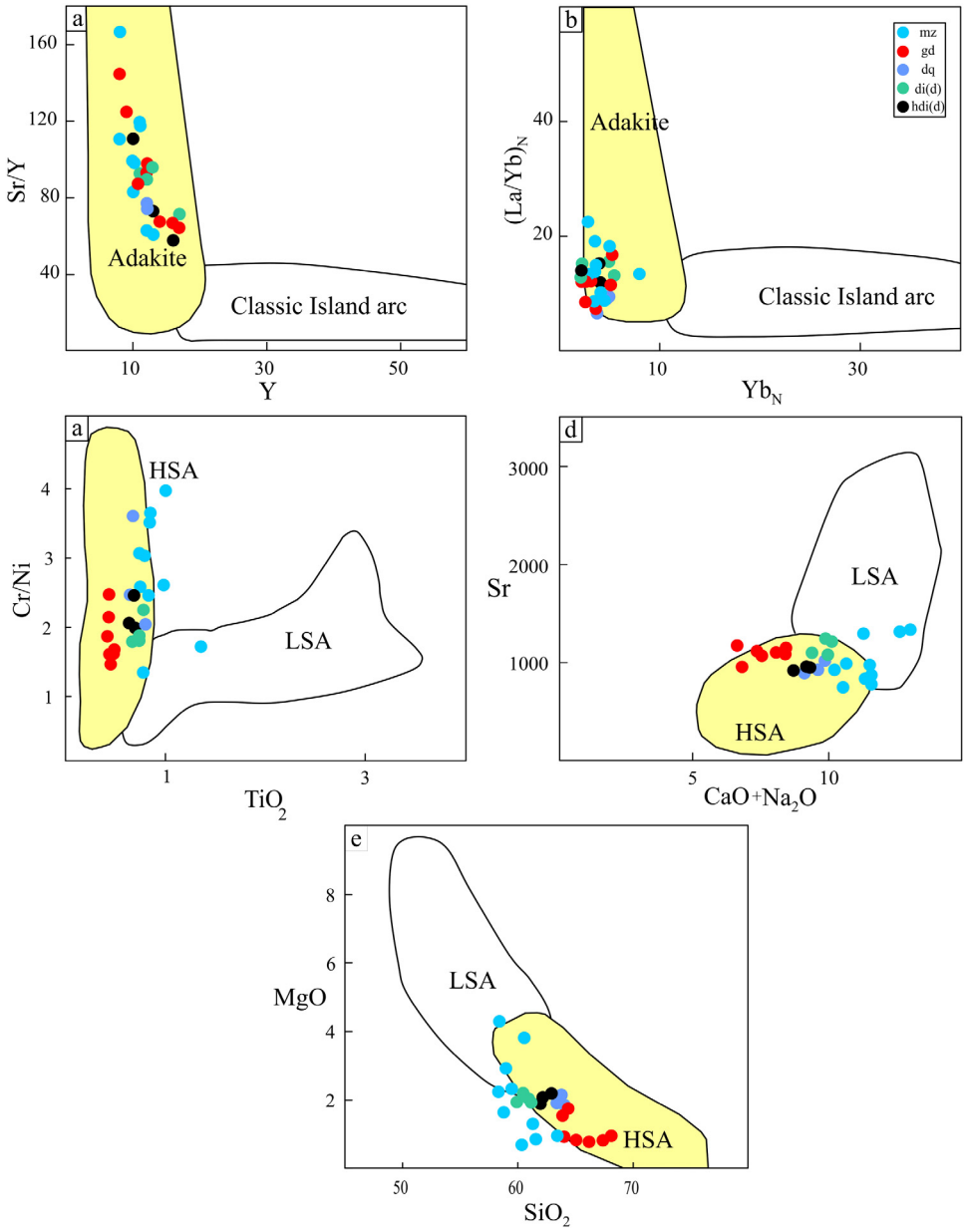


**Fig. 6.** (a) and (b) Diagrams for discriminating adakitic magmas from mantle-derived magmas (Defant and Drummond, 1990), (c) Cr/Ni vs. $TiO_2$ diagram, (d) Sr vs. $CaO + Na_2O$ diagram, (e) MgO–$SiO_2$ diagram (Martin et al., 2005) to distinguish high-silica and low-silica adakites (sample symbols as Table 1).

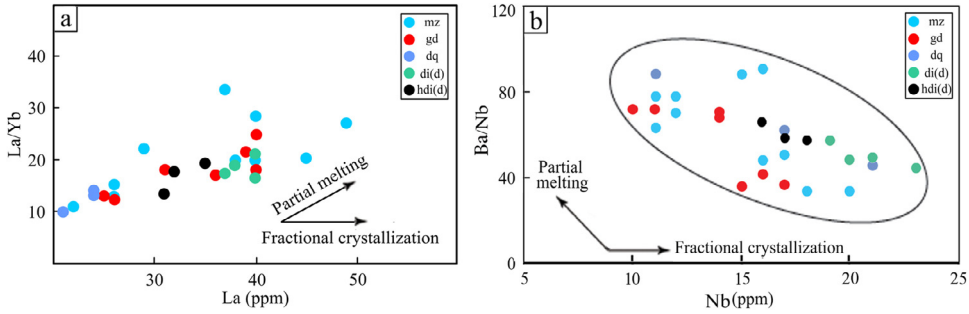


**Fig. 7.** (a) La/Yb vs. La, and (b) Ba/Nb vs. Nb (Bourdon et al., 2002) plots, revealing a partial melting trend for the analyzed intrusive rocks (sample symbols as Table 1).

magmas in the mantle wedge. Additionally, U enrichment in spider diagrams can indicate the incorporation of pelagic sediments and or altered oceanic crust in the magma generation (Fan et al., 2003).

Finally, the lack of negative P, Sr, Ba and Eu anomalies testifies to the fact that the studied plutonic complex cannot be originated from continental crust, as the lack of such negative anomalies indi-

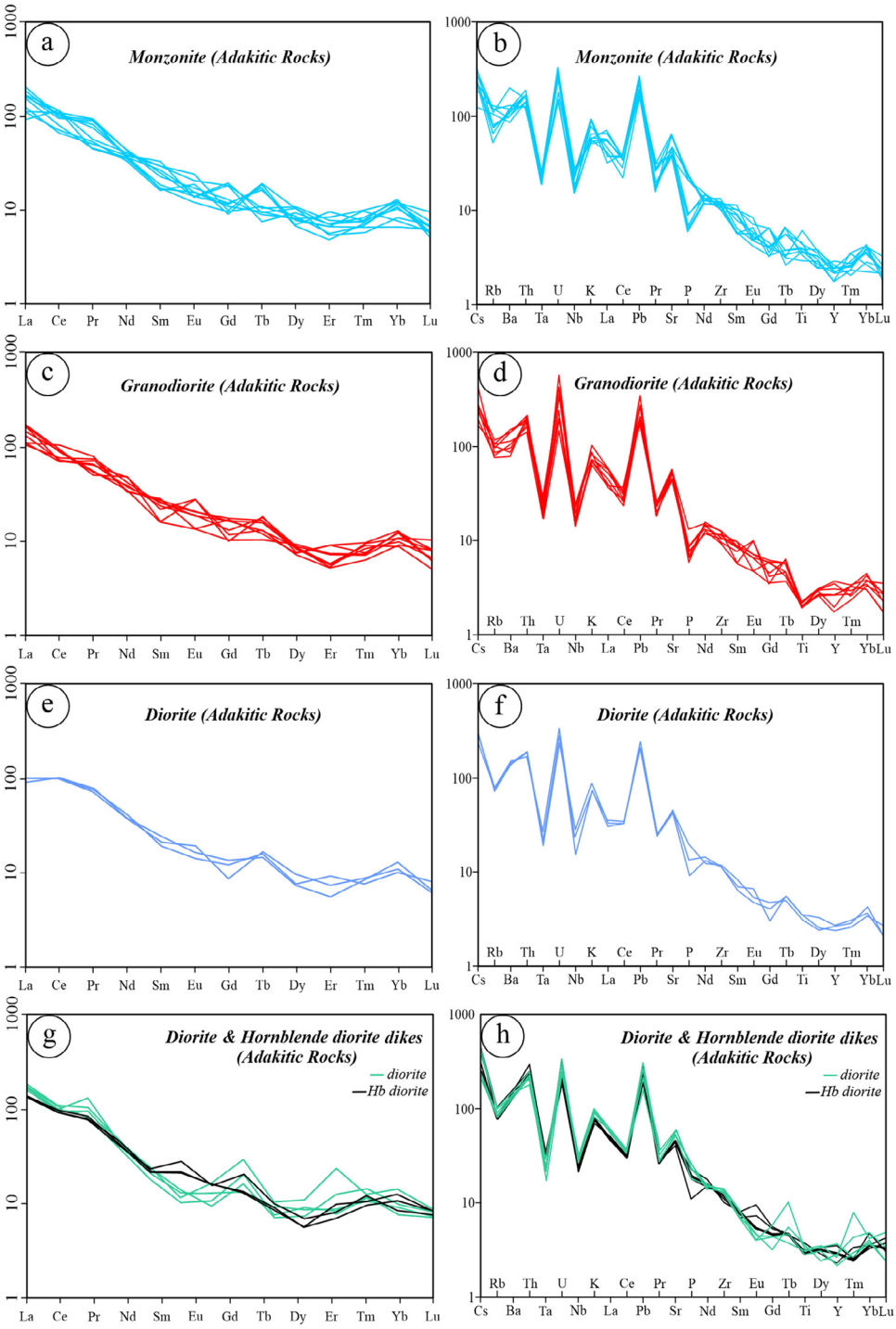


**Fig. 8.** (a), (c), (e), (g) Chondrite-normalized (McDonough and Sun, 1995) rare earth element distribution patterns, and (b), (d), (f), (h) Primitive mantle-normalized (Sun and McDonough, 1989) trace and rare earth elements distribution patterns for monzonitic, granodioritic, dioritic rocks and the cross-cutting dioritic dikes, respectively.

cates the lack of crystal fractionation and partial melting of the lower continental crust (Pe-Piper et al., 2002).

### 4.3. Petrogenesis of the studied plutonic bodies

As it was mentioned earlier, adakites are commonly found in subduction zones (Prouteau et al., 2001; Martin et al., 2005; Moyen, 2009), being related to the hot and young (10–25 Ma) oceanic crusts or ridges and show close similarity with experimental mafic magmas (Martin et al., 2005; Rapp and Watson, 2007). HSAs are produced by the melting of mafic rocks of subducted oceanic crust under high pressure (garnet stability field = eclogite and garnet amphibolite facies), whereas LSAs are resulted from partial melting of the mantle wedge peridotite, which is already metasomatized through the reaction with slab melts and undergone compositional changes. Partial melting of the mafic protores is only possible in the amphibolite to eclogite transitional facies, under the minimum pressure between 15 and 25 kb and temperatures ranging from 700 to 900 °C.

However, magmas in the subduction zones can also be derived from sediments overlying the subducting oceanic slab, the lower mafic continental crust (e.g., Atherton and Petford, 1993; Rollinson

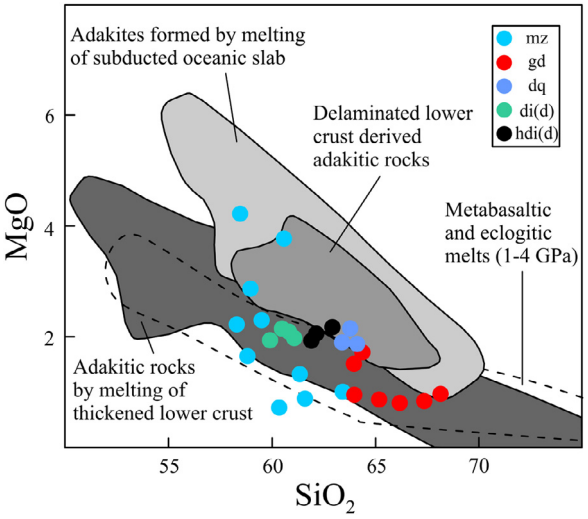


**Fig. 9.** MgO vs. $SiO_2$ diagram (Karsli et al., 2011 and references therein) and the plotted data points (sample symbols as Table 1).

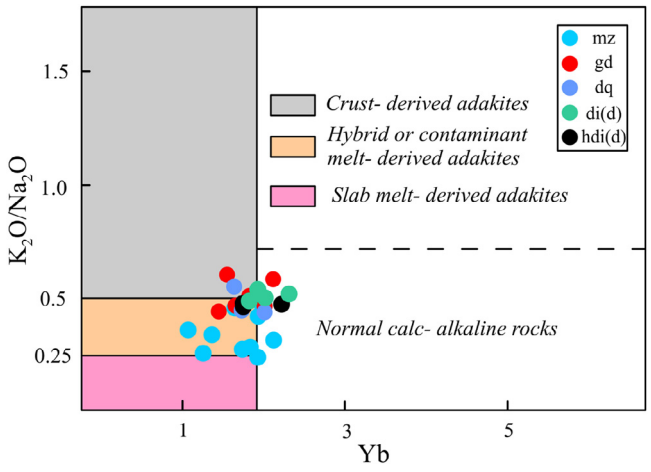


**Fig. 11.** $K_2O/Na_2O$ vs. Yb diagram to distinguish the source of adakitic rocks (Kamvong et al., 2014) (sample symbols as Table 1).

and Tarney, 2005), as well as a mixture of all these sources along with differentiation, assimilation and contamination processes. Additionally, magmas are also reported to be formed in post-collisional settings (Xu et al., 2006) through melting of the lower crust under the influence of the intruding deeply-originated K-enriched magmas.

In order to determine the source of adakitic rocks in the studied area, the MgO–$SiO_2$ diagram (Karsli et al., 2011) was used (Fig. 9). The plotted data points lie in the overlapping area of adakites derived from metabasaltic and eclogitic melts and the field of adakites derived from melting of the thickened lower crust. Meanwhile, based on Th–$K_2O$ and Ni–$SiO_2$ plots (Fig. 10a and b; Eyuboglu et al., 2012), the adakitic rocks of the Khoynarood are plotted in the overlapping area of adakites derived from subducting oceanic crust (Wang et al., 2006a), adakites originated from delaminated lower continental crust (Xu et al., 2002; Gao et al., 2004; Wang et al., 2004; Wang et al., 2006a; Wang et al., 2006b) and early Cenozoic adakites derived through a slab window (Eyuboglu et al., 2011a,b). However, delaminated lower crust produces melts with high Th and Th/La values (Plank, 2005), whereas these values are low in the analyzed samples, ruling out their origination from the delaminated lower crust. Based on Fig. 11, adakites derived from continental crust tend to have higher $K_2O/Na_2O$ ratios, which may be resulted from incorporation of the felsic continental rocks. Alteration processes can also be involved. This ratio is low in the studied adakites, but is still higher than the initial slab melts, ranging between 0.25 and 0.5 in most samples. Accordingly, most of the samples are plotted in hybrid or contaminated melt-derived adakites field (Fig. 11).

To conclude, by taking into account the low Th (11–25 ppm) and Th/La values (0.24–0.8) of the studied rocks, $SiO_2$ and $TiO_2$ contents (>59.1 and <0.81 wt.%, respectively), as well as their $K_2O/Na_2O$ ratio and their high-silica type characteristics, it can be inferred that partial melting of the subducting oceanic crust (in this case, the Neo-Tethyan oceanic crust) was most likely responsible for the generation of adakitic magmatism in the study area as part of the UDMA. Magmas generated through partial melting of the subducted slab or its overlying sediments are characterized by high Sr/Ce ratio, with Nb/Zr ratio above 0.04 (Elburg et al., 2002). The average of Nb/Zr and Sr/Ce ratios of the studied samples are 0.12 and 18, respectively, testifying to the role of the subducting slab in parental magma generation.

Based on the Th/Yb vs. Th/Sm diagram (Fig. 12a; Zhu et al., 2009), the Khoynarood samples show close relationship with the post collisional adakites reported from Tibet (Chung et al., 2003; Hou et al., 2004; Guo et al., 2007), while in the Th/Ce vs. Th diagram (Fig. 12b; Wang et al., 2008) to discriminate the tectonic setting of adakites, the data points plot within the post-collisional field. These

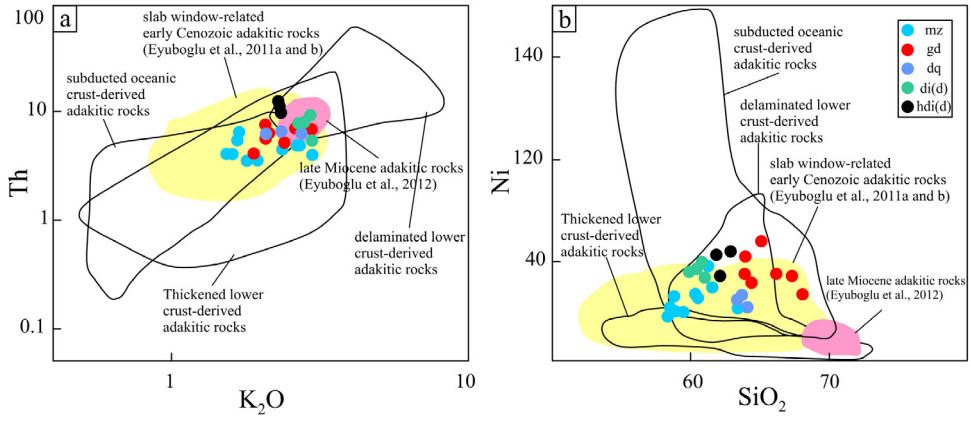


**Fig. 10.** (a) Th–$K_2O$ and (b) Ni–$SiO_2$ diagrams to discriminate the source of the adakitic rocks (Eyuboglu et al., 2012) (sample symbols as Fig. 4). Subducted oceanic crust-derived adakites field from Wang et al. (2006a); Delaminated lower crust-derived adakites field from Gao et al. (2004), Wang et al. (2004, 2006a, 2006b) Xu et al. (2002); Thick lower-crust derived adakites field from Atherton and Petford (1993), Johnson et al. (1997), Muir et al. (1995), Petford and Atherton (1996) (sample symbols as Table 1).

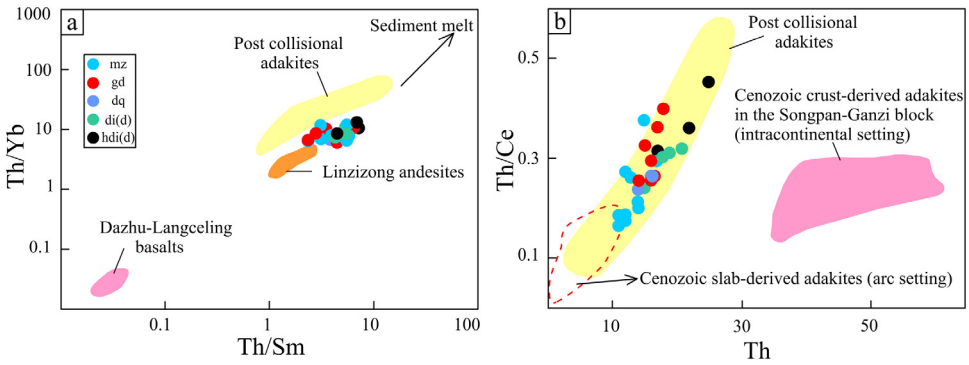


**Fig. 12.** (a) Th/Yb vs. Th/Sm (Zhu et al., 2009) and (b) Th/Ce–Th (Wang et al., 2008) diagrams for discriminating the source and the tectonic setting of the studied adakitic rocks, where the fields of post-collisional adakites (Chung et al., 2003), Linzizong andesites (Mo et al., 2007), Cenozoic crust-derived adakites of Songpan–Ganzi block (intercontinental setting) and Cenozoic slab-derived adakites (arc setting; Hou et al., 2004; Guo et al., 2007; Wang et al., 2008) are shown (sample symbols as Table 1).

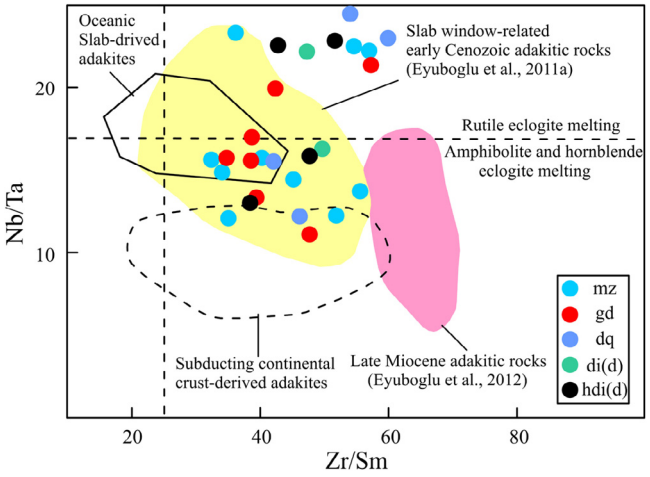


**Fig. 13.** Nb/Ta vs. Zr/Sm variation diagram (Condie, 2005; Wang et al., 2008; Eyuboglu et al., 2012) (sample symbols as Table 1).

results, along with Fig. 5b, testify to the post-collisional nature of the studied intrusive rocks.

Investigations show that partial melting of metabasaltic igneous rocks in the garnet amphibolite to eclogite facies can lead to generation of melts with adakitic characteristics (Defant and Drummond, 1990; Guo et al., 2007; Wang et al., 2008). Based on the high Sr content of the studied rocks and the lack of negative Eu anomaly, it can be perceived that plagioclase was not left behind at the source area as a residual phase, while the depletion of Nb and Ti testifies to the presence of rutile and/or amphibole as residues in the source materials, probably provoking a garnet-amphibolite and/or amphibole eclogite source.

To distinguish between the eclogitic and garnet-amphibolitic source materials, it must be noted that, unlike an amphibolitic source, melting of eclogitic materials produces much higher Nb/Ta ratios ($14 \pm 4$) due to the presence of rutile (Foley et al., 2002; Schmidt et al., 2004). The average Nb/Ta ratio of the studied rocks is about 17.85 (10.91–30.0), testifying to an eclogitic source and the data points plot within the rutile-bearing and amphibole-bearing eclogite fields in Fig. 13. The presence and remaining of amphibole within the eclogitic source rocks is conceivable from the spoon-like distribution pattern of REEs (Fig. 8). The plotted data points also correlate well with the slab window-related early Cenozoic adakitic rocks field delineated by Eyuboglu et al. (2011a), while also show affinities towards the oceanic slab-derived adakites.

At the end, it is noteworthy to mention that post-collisional ultra −potassic (Saray Peninsula) and alkaline basaltic lavas of the late Miocene and Plio-Quaternary (respectively) in NW Iran are attributed to the partial melting of the enriched and metasomatized mantle followed by slab break-off and development of an asthenospheric window, which facilitated partial melting of the subduction-contaminated lithospheric mantle and resulted in the formation of high-K and alkaline lavas through low-degree partial melting (e.g., Shafaii Moghadam et al., 2014). Such basaltic lavas are also found in the study area (Fig. 2).

### 4.4. Geodynamic setting

To summarize all the presented discussions, the geochemical features of the studied rocks imply to a low-degree partial melting of a hydrous and mainly eclogitic source, most likely the subducting oceanic slab at high pressure, which could favorably converted to the amphibole-eclogite facies, leaving behind a residual assemblage rich in hornblende and garnet with less or no plagioclase.

Based on the seismic tomography studies, a large low-velocity anomaly has been reported beneath the UDMA (Maggi and Priestly, 2005). Such a phenomenon can probably be resulted from ascending of the asthenospheric mantle beneath this region. In order to explain and interpret this phenomenon, various mechanisms such as detachment of the subducting oceanic slab (Ghasemi and Talbot, 2006; Omrani et al., 2008) or its retardation (Morley et al., 2009) have been proposed. Jahangiri (2007) and Simmonds (2013) conclude that adakitic magmatism in NW Iran has occurred after the termination of the subduction in the Neo-Tethyan basin at early Cenozoic, following the slab break-off and upwelling of the asthenosphere in the slab window, which could trigger the partial melting of the detached slab; This scenario can also be considered for the studied intrusions as well. In this regard, after the collision of the Arabian and Central Iranian plates during the late Cretaceous–early Paleocene (Ghalamghash et al., 2009; Mazhari et al., 2009) to Eocene (Ghasemi and Talbot, 2006; Omrani et al., 2008), the oceanic slab break-off has happened and asthenosphere has ascended through the slab window (e.g., Shafaii Moghadam et al., 2014), leading to an increase in the thermal gradient. Meanwhile, melting of the detached slab has produced HSA adakitic magmatism along the UDMA belt, as well as in East Turkey. Lack of LSA characteristics among the studied magmatic rocks of this belt, especially in NW Iran, is against the partial melting of the metasomatized mantle wedge peridotite, though interaction of the slab-derived magma with the mantle wedge peridotite is evident. On the other hand, the presented plots and the compositional characteristics of the studied rocks (e.g., lack of K enrichment and very high amounts of incompatible elements such as Ba, Rb and Th; Wang et al., 2008), as well as the evidence provided by Simmonds (2013) against the melting of thickened lower crust for the mag-

matic rocks of Kighal area (some 12 km southeast of Khoynarood) rule out the partial melting of the lower mafic crust under the influence of ascending asthenospheric mantle. Nevertheless, to provide meaningful constraints on petrogenesis and geodynamics of these intrusions, precise radiometric dating and stable isotope studies seem necessary.

## 5. Conclusions

The intrusive bodies of the Khoynarood are located in NW Iran and are part of the Tertiary Urumieh–Dokhtar Magmatic Arc. Their composition ranges from monzonite, through granodiorite to diorite–quartz diorite and they are cross-cut by dioritic and hornblend-dioritic dike swarms. They have moderate to high $K_2O$ content and based on the discriminating diagrams for tectonic setting, the studied rocks show post-collisional setting.

According to the geochemical data obtained for the studied rocks and the La/Yb–Yb and Sr/Y–Y diagrams, they have adakitic characteristics, corresponding to high-silica adakites. The chondrite- and primitive mantle-normalized distribution patterns of trace and rare earth elements reveal enrichment of the LREEs and LILEs and depletion of HREEs and HFSEs, as well as negative anomalies of Nb, Ta and Ti in the studied rocks. The low HREE and Y contents can be attributed to the presence of garnet and amphibole (the latter is further manifested by the concave distribution pattern of the REEs) as residual phases within the source region.

In various discriminating diagrams proposed to determine the source and petrogenesis of adakitic rocks, there is a considerable overlap between different adakites produced by slab or continental crust melting. Most of the data points plot in this overlapping part of the fields of adakites with different sources. However, based on the discussions presented in this paper, the most likely scenario for the studied adakitic intrusions is their origination form the low-degree partial melting of the subducted Neo-Tethyan oceanic crust under conditions which could provide amphibole eclogite facies, leaving behind a residual assemblage rich in hornblende and garnet with less or no plagioclase, in the same way as the other adakitic rocks of NW Iran. However, considering the lack of isotopic data, acceptance of a specific mechanism for the genesis of studied adakites should be with caution.

By considering the termination of the Neo-Tethyan oceanic crust subduction at upper Cretaceous and the relative age of the studied intrusions (Oligocene), it is perceivable that the generation of HSA-type adakitic rocks in Khoynarood was resulted from detachment of the subducting slab after subduction cessation (which most likely experienced eclogite facies conditions) and the partial melting of the detached slab due to the thermal perturbation. Consequently, slab-derived magma underwent interactions with mantle wedge peridotite and continental crust during its ascending, which is manifested by the geochemical composition of the related rocks in the area.

## Acknowledgements

This study was financially supported by the Khoynarood Base Metal Company. Therefore, the authors would like to express their thanks and appreciation to this company and its managing director Rasoul Alizadeh. The authors are also indebted to the two anonymous reviewers and the editor of the journal for their constructive comments and suggestions, which greatly helped to improve the manuscript. Thanks are also extended to Masood Baghban for his cooperation during this study.

## References

Agard, P., Omrani, J., Jolivet, L., Mouthereau, F., 2005. Convergence history across Zagros (Iran): constraints from collisional and earlier deformation. Inter. J. Earth Sci. (Geol. Rundsch.) 94, 401–419.
Aghanabati, A., 2004. Geology of Iran. Geological Survey of Iran, Tehran (in Persian).
Aghazadeh, M., Castro, A., Rashidnezhad Omran, N., Emami, H., Moinvaziri, H., Badrzadeh, Z., 2010. The gabbro (shoshonitic)-monzonite-granodiorite association of mountains Khankandi pluton, Alborz Mountains, NW Iran. J. Asian Earth Sci. 38, 199–219.
Aghazadeh, M., Emami, M.H., Moinvaziri, H., Rashidnezhad Omran, N., Castro, A., 2011. Post-collisional shoshonitic, C-type adakitic and lamprophyric plutonism in the pluton Khankandi Pluton, Arasbaran (NW Iran). Geosci. 20, 167–172 (in Persian).
Almeida, M.E., Macambira, M.J.B., Oliveira, E.C., 2007. Geochemistry and zircon geochronology of the I-type high-K calc-alkaline and S-type granitoid rocks from southeastern Roraima, Brazil: Orosirian collisional magmatism evidence (197-1.96 Ga) in central portion of Guyana Shield. Precambrian Res. 155, 69–97.
Amidi, S.M., Emami, M.H., Michel, R., 1984. Alkaline character of Eocene volcanism in the middle part of Iran and its geodynamic situation. Inter. J. Earth Sci. 73, 917–932.
Arslan, M., Aslan, Z., 2006. Mineralogy, petrography and whole-rock geochemistry of the Tertiary Granitic Intrusions in the Eastern Pontides, Turkey. J. Asian Earth Sci. 27, 177–193.
Atherton, M.P., Petford, N., 1993. Generation of sodium-rich magmas from newly underplated basaltic crust. Nature 362, 144–146.
Azizi, H., Moinevaziri, H., 2009. Review of the tectonic setting of Cretaceous to Quaternary volcanism in northwestern Iran. J. Geodyn. 47, 167–179.
Barnes, C.G., Petersen, S.W., Kistler, R.W., Murray, R., Kays, M.A., 1996. Source and tectonic implications of tonalite-trondhjemite magmatism in the Klamath Mountains. Contrib. Mineral. Petr. 123, 40–60.
Berberian, M., King, G.C.P., 1981. Towards a paleogeography and tectonic evolution of Iran. Can. J. Earth Sci. 18, 210–265.
Bourdon, E., Eissem, J.-P., Monzier, M., Robin, C., Martin, H., Cotton, J., Hall, M.L., 2002. Adakite-like lavas from Antisana Volcano (Ecuador): evidence for slab melt metasomatism beneath the Andean northern volcanic zone. J. Petrol. 43, 199–217.
Brunet, M.F., Korotaev, M.V., Ershov, A.V., Nikishin, A.M., 2003. The South Caspian Basin: a review of its evolution from subsidence modeling. Struct. Geol. 156, 119–148.
Castillo, P.R., Janney, P.E., Solidum, R.U., 1999. Petrology and geochemistry of Camiguin Island: southern Philippines: insights to the source of adakites and other lavas in a complex arc setting. Contrib. Mineral. Petr. 134, 33–51.
Chung, S.L., Liu, D.Y., Ji, J.Q., Chu, M.F., Lee, H.Y., Wen, D.J., Lo, C.H., Lee, T.Y., Qian, Q., Zhang, Q., 2003. Adakites from continental collision zones: melting of thickened lower crust beneath southern Tibet. Geology 31, 1021–1024.
Condie, K.C., 2005. TTG's and adakites: are they both slab melts? Lithos 80, 33–44.
Cox, K.G., Bell, J.D., Pankhurst, R.J., 1979. The Interpretation of Igneous Rocks. George Allen and Unwin.
Danyushevsky, L.V., Falloon, T.J., Crawford, A.J., Tetroeva, S.A., Leslie, R.L., Verbeeten, A., 2008. High-Mg adakites from Kadavu Island Group, Fiji, southwest Pacific: evidence for the mantle origin of adakite parental melts. Geology 36, 499–502.
Defant, M.J., Drummond, M.S., 1990. Derivation of some modern arc magmas by melting of young subducted lithosphere. Nature 347, 662–665.
Ding, L., Kapp, P., Yue, Y., Lai, Q., 2007. Post-collisional calc-alkaline lavas and xenoliths from the Southern Qiangtang terrain, central Tibet. Earth Planet. Sci. Lett. 254, 28–38.
Elburg, M.A., Bergen, M., Hoogewerff, J., Vroon, P., Zulkarnain, I., Nasution, A., 2002. Geochemical trends across an arc-continent collision zone: magma sources and slab-wedge transfer processes below the Pantar Strait volcanoes, Indonesia. Geochim. Comochim. Acta 66, 2771–2789.
Eyuboglu, Y., Chung, S.L., Santosh, M., Dudas, F.O., Akaryali, E., 2011a. Transition from shoshonitic to adakitic magmatism in the Eastern Pontides, NE Turkey: implications for slab window melting. Gondwana Res. 19, 413–429.
Eyuboglu, Y., Santosh, M., Dudas, F.O., Chung, S.L., Akaryali, E., 2011b. Migrating magmatism in a continental arc: geodynamics of the Eastern Mediterranean revisited. J. Geodyn. 52, 2–15.
Eyuboglu, Y., Santosh, M., Yi, K., Bektaş, O., Kwon, S., 2012. Discovery of Miocene adakitic dacite from the Eastern Pontides belt and revised geodynamic model for the late Cenozoic evolution of eastern Mediterranean region. Lithos 146–147, 218–232.
Eyuboglu, Y., Santosh, M., Dudas, O.F., Akaryali, E., Chung, S.L., Akdag, K., Bektas, O., 2013. The nature of transition from adakitic to non-adakitic magmatism in a slab window setting: a synthesis from the eastern Pontides, NE Turkey. Geosci. Front. 4, 353–375.
Fan, W.M., Gue, F., Wang, Y.J., Lin, G., 2003. Late Mesozoic calc-alkaline volcanism of post-orogenic extention in the northen Da Hinggan Mountains, northeastern China. J. Volcanol. Geoth. Res. 121, 115–135.
Foley, S.F., Tiepolo, M., Vannucci, R., 2002. Growth of early continental crust controlled by melting of amphibolite in subduction zones. Nature 417, 837–840.
Gao, S., Rudnick, R.L., Yuan, H.L., Liu, X.M., Xu, W.L., Lin, W.L., Ayers, J., Wang, X.C., Wang, Q.H., 2004. Recycling lower continental crust in the North China Craton. Nature 432, 892–897.

Gao, Y., Hou, Z., Kamber, B.S., Wei, R., Meng, X., Zhao, R., 2007. Adakite-like porphyries from the southern Tibetan continental collision zones: evidence for slab melt metasomatism. Contrib. Mineral. Petr. 153, 105–120.
Ghalamghash, J., Nedelec, A., Bellon, B., Vousoughi Abedini, M., Bouchez, J.L., 2009. The Urumieh plutonic complex (NW Iran): a record of the geodynamic evolution of the Sanandaj-Sirjan zone during Cretaceous times, Part I: Petrogenesis and K/Ar dating. J. Asian Earth Sci. 35, 401–415.
Ghasemi, A., Talbot, C.J., 2006. A new tectonic scenario for the Sanandaj-Sirjan Zone (Iran). J. Asian Earth Sci. 26, 683–693.
Glennie, K.W., 2000. Cretaceous tectonic evolution of Arabia's Eastern plate margin: a tale of two oceans. SEPM Sp. Pub. 69, 9–20.
Green, N.L., Harry, D.L., 1999. On the relationship between subducted slab age and arc basalt petrogenesis Cascadia subduction system. North Am. Earth Planet. Sci. Lett. 171, 367–381.
Grove, T.L., Baker, M.B., Price, R.C., Parman, S.W., Elkins-Tanton, L.T., Chatterjee, N., Muntener, O., 2005. Magnesian andesite and dacite lavas from Mt. Shasta, northern California: products of fractional crystallization of $H_2O$-rich mantle melts. Contrib. Mineral. Petr. 148, 542–565.
Guo, Z.F., Wilson, M., Liu, J.Q., 2007. Post-collisional adakites in south Tibet: products of partial melting of subduction-modified lower crust. Lithos 96, 205–224.
Hajialioghli, R., Moazzen, M., 2014. Supra-subduction and mid-ocean ridge peridotites from the Piranshahr area, NW Iran. J. Geodyn. 81, 41–55.
Horton, B.K., Hassanzadeh, J., Stockli, D.F., Axen, G.J., Gillis, R.J., Guest, B., Amini, A., Fakhari, M.D., Zamanzadeh, S.M., Grove, M., 2008. Detrital zircon provenance of Neoproterozoic to Cenozoic deposits in Iran: implications for chronostratigraphy and collisional tectonics. Tectonophysics 451, 97–122.
Hou, Z.Q., Gao, Y.F., Qu, X.M., Rui, Z.Y., Mo, X.X., 2004. Origin of adakitic intrusives generated during mid-Miocene east-west extension in southern Tibet. Earth Planet. Sci. Lett. 220, 39–155.
Jahangiri, A., Ahmadzadeh, G., Lentz, D., 2011. Crystal chemistry of phlogopite minerals from Plio-Quaternary potassic volcanic rocks, NW Iran. Iran. J. Cryst. Mineral. 19, 399–412 (in Persian).
Jahangiri, A., 2007. Post-collisional Miocene adakitic volcanism in NW Iran: geochemical and geodynamic implications. J. Asian Earth Sci. 30, 433–447.
Johnson, K., Barnes, C.G., Miller, C.A., 1997. Petrology, geochemistry, and genesis of high-Al tonalite and trondhjemites of the Cornucopia stock, Blue Mountains, Northeastern Oregon. J. Petrol. 38, 1585–1611.
Kamvong, T., Zaw, K., Meffre, S., Maas, R., Stein, H., Lai Ch, K., 2014. Adakites in the Truong Son and Loei fold belts, Thailand and Laos: genesis and implications for geodynamics and metallogeny. Gondwana Res. 26, 165–184.
Karsli, O., Ketenchi, M., Uysal, I., Dokuz, A., Aydin, F., Chen, B., Kandemir, R., Wijbrans, J., 2011. Adakite-like granitoid porphyries in the Eastern Pontides, NE Turkey: potential parental melts and geodynamic implications. Lithos 127, 354–372.
Kay, R.W., 1978. Aleutian magnesian andesites: melts from subducted Pacific ocean crust. J. Volcanol. Geoth. Res. 4, 117–132.
Keppler, H., 1996. Constraints from partitioning experiments on the composition of subduction zone fluids. Nature 380, 237–240.
Lustrino, M., Keskin, M., Mattioli, M., Iebedev, V.A., Chugaev, A., Sharkov, E., Kavak, O., 2010. Primordial activity of the largest Cenozoic shield volcano of the Circum-Mediterranean Mt. Karacadag, SE Turkey. Euro. J. Mineral. 22, 343–362.
Lustrino, M., Keskin, M., Mattioli, M., Kavak, O., 2012. Multiple sources feeding the volcanic activity of Mt: Karacadag (SE Turkey). J. Asian Earth Sci. 46, 120–139.
Macpherson, C.G., Dreher, S.T., Thirlwall, M.F., 2006. Adakites without slab melting: high pressure differentiation of island arc magma, Mindanao, the Philippines. Earth Planet. Sci Lett. 243 (3–4), 581–593.
Maggi, A., Priestly, K., 2005. Surface waveform tomography of the Turkish-Iranian plateau. Geophys. J. Inter. 160, 1068–1080.
Martin, H., Smithies, R.H., Moyen, Rapp, Champion, J.-F., 2005. An overview of adakite, tonalite-tronjomite-granodiorite (TTG), and sanukitoid: relationships and some implications for crustal evolution. Lithos 79, 1–24.
Martin, H., 1999. Adakitic magmas: modern analogues of Archaean granitoids. Lithos 46, 411–429.
Mazhari, S.A., Bea, F., Amini, S., 2009. The Eocene bimodal Piranshahr massif of the Sanandaj-Sirjan Zone, NW Iran: a marker of the end of the collision in the Zagros orogeny. J. Geol. Soc. Lond. 166, 1–17.
McDonough, W.F., Sun, S.-S., 1995. The composition of the Earth. Chem. Geol. 120, 223–253.
Mehrpartou, M., Amini Fazl, A., Radfar, J., 1992. 1:100000 Geologic Map of Varzeghan. Geological Survey of Iran.
Mo, X.X., Hou, Z.Q., Niu, Y.L., Dong, G.C., Qu, X.M., Zhao, Z.D., Yang, Z.M., 2007. Mantle contributions to crustal thickening during continental collision: evidence from Cenozoic igneous rocks in southern Tibet. Lithos 96, 225–242.
Mohajjel, M., Fergusson, C.L., 2000. Dextral transpression in late Cretaceous continental collision, Sanandaj-Sirjan zone, western Iran. J. Struct. Geol. 22, 1125–1139.
Morley, C.K., Kongwung, B., Julapour, A.A., Abdolghafourian, M., Hajian, M., Waples, D., Warren, J., Otterdoom Srisuriyon, H.K., Kazemi, H., 2009. Structural development of a major late Cenozoic basin and transpressional belt in central Iran: the Central Basin in the Qom-Saveh area. Geosphere 50, 325–362.
Moyen, J.-F., 2009. High Sr/Y and La/Yb ratios: the meaning of the adakitic signature. Lithos 112, 556–574.
Muir, R.J., Weaver, S.D., Bradshaw, J.D., Eby, G.N., Evans, J.A., 1995. Geochemistry of the Cretaceous Separation Point Batholith, New Zealand: granitoid magmas formed by melting of mafic lithosphere. J. Geol. Soc. Lond. 152, 689–701.
Nabavi, M.H., 1976. An introduction to the Geology of Iran, 1976, Geological Survey of Iran. Geological Survey of Iran, Tehran (in Persian).
Nicholson, K.N., Black, P.M., Hoskin, P.W.O., Smith, I.E.M., 2004. Silicic volcanism and back arc extension related to migration of the late Cenozoic Australian-Pacific plate boundary. J. Volcanol. Geoth. Res. 131, 295–306.
Omrani, J., Agard Ph Whitechurch, H., Benoit, M., Prouteau, G., Jolivet, L., 2008. Arc magmatism and subduction history beneath the Zagros Mountains, Iran: a new report of adakites and geodynamic consequences. Lithos 106, 380–398.
Pang, K.N., Chung, S.L., Zarrinkoub, M.H., Li, X.H., Lee, H.Y., Lin, T.H., Chiu, H.Y., 2016. New age and geochemical constraints on the origin of Quaternary adakite-like lavas in the Arabia-Eurasia collision zone. Lithos 264, 348–359.
Pe-Piper, G., Piper, D.J.W., Matarangas, D., 2002. Regional implications of geochemistry and style of emplacement of Miocene I-type diorite and granite Delos, Cyclades, Greece. Lithos 60, 47–66.
Pearce, J.A., Harris, N.B.W., Tindle, A.G., 1984. Trace element discrimination diagrams for the tectonic interpretation of granitic rocks. J. Petrol. 25, 956–983.
Pearce, J.A., 1996. Source and setting of granitic rocks. Episodes 19, 120–125.
Petford, N., Atherton, M., 1996. Na-rich partial melting from newly underplated basaltic crust: the Cordillera Blanca Batholith, Peru. J. Petrol. 37, 1491–1521.
Plank, T., 2005. Constraints from Thorium/Lanthanum on sediment recycling at subduction zones and the evolution of the continents. J. Petrol. 46, 921–944.
Prouteau, G., Scaillet, B., 2003. Experimental constraints on the origin of the 1991 Pinatubo dacite. J. Petrol. 44, 2203–2241.
Prouteau, G., Scaillet, B., Pichavant, M., Maury, R., 2001. Evidence for mantle metasomatism by hydrous silicic melts derived from subducted oceanic crust. Nature 410, 197–200.
Rapp, R.P., Watson, E.B., 2007. Dehydration melting of metabasalt at 8–32 kbar: implications for continental growth and crust-mantle recycling. J. Petrol. 36, 891–931.
Rapp, R., Xiao, L., Shimizu, N., 2002. Experimental constraints on the origin of potassium-rich adakites in eastern China. Acta Petrol. Sin. 18, 293–302.
Richards, J.R., Kerrich, R., 2007. Adakite-like rocks: their diverse origins and questionable role in metallogenesis. Econ. Geol. 102, 537–576.
Rickwood, P.C., 1989. Boundary lines within petrologic diagrams which use oxides of major and minor elements. Lithos 22, 247–263.
Robin, C., Eissen, J.P., Samaniego, P., Martin, H., Hall, M., Cotton, J., 2009. Evolution of the late Pleistocene Mojanda-Fuya volcanic complex (Ecuador), by progressive adakitic involvement in mantle magma sources. Bull. Volcanol. 71, 233–258.
Rollinson, H.R., 1993. Using Geochemical Data: Evaluation, Presentation, Interpretation. Longman Scientific and Technical, Wiley New York.
Rollinson, H.R., Tarney, J., 2005. Adakites – the key to understanding LILE depletion in granulites. Lithos 79, 61–81.
Saccani, E., Azimzadeh, Z., Dilek, Y., Jahangiri, A., 2013. Geochronology and petrology of the early Carboniferous Misho Mafic Complex (NW Iran), and implications for the melt evolution of Paleo-Tethyan rifting in Western Cimmeria. Lithos 162–163, 264–278.
Schandl, E.S., Gorton, M.P., 2002. Application of high field strength elements to discriminate tectonic settings in VMS environments. Econ. Geol. 97, 629–642.
Schmidt, M.W., Dardon, A., Chazot, G., Vannucci, R., 2004. The dependence of Nb and Ta rutile-melt partitioning on melt composition and Nb/Ta fractionation during subduction processes. Earth Planet. Sci. Lett. 226, 415–432.
Shafaii Moghadam, H., Ghorbani, G., Zaki Khedr, M., Fazlnia, N., Chiaradia, M., Eyuboglu, Y., Santosh, M., Galindo Francisco, C., Lopez Martinez, M., Gourgaud, A., Arai, S., 2014. Late Miocene K-rich volcanism in the Eslamieh peninsula (Saray), NW Iran: implications for geodynamic evolution of the Turkish-Iranian high plateau. Gondwana Res. 26, 1028–1050.
Sheth, H.C., Torres-Alvarado, I.S., Verma, S.P., 2002. What is the calc-alkaline rock series? Inter. Geol. Rev. 44, 686–701.
Simmonds, V., 2013. Geochemistry and petrogenesis of an adakitic quartz monzonitic porphyry rock and related cross-cutting dike suites, Kighal, northwest Iran. Inter. Geol. Rev. 55, 1126–1144.
Sun, S.S., McDonough, W.F., 1989. Chemical and isotopic systematic of oceanic basalts: implications for mantle composition and processes. In: Saunders, A.D., Norry, M.J. (Eds.), Magmatism in Ocean Basins, 42. Geol. Soc., London, pp. 313–345.
Wang, Q., Xu, J.F., Zhao, Z.H., Bao, Z.W., Xu, W., Xiong, X.L., 2004. Cretaceous high-potassium intrusive rocks in the Yueshan?Hongzhen area of east China: adakites in an extensional tectonic regime within a continent. Geochem. J. 38, 417–434.
Wang, Q., Derek, A.W., Xu, J.F., Zhao, Z.H., Jian, P., Xiong, X.L., Bao, Z.W., Li, C.F., Bai, Z.H., 2006a. Petrogenesis of Cretaceous adakitic and shoshonitic igneous rocks in the Luzong area, Anhui Province (eastern China): implications for geodynamics and Cu-Au mineralizations. Lithos 89, 424–446.
Wang, Q., Xu, J.F., Jian, P., Bao, Z.W., Zhao, Z.H., Li, C.F., Xiong, X.L., Ma, J.L., 2006b. Petrogenesis of adakitic porphyries in an extensional tectonic setting, Dexing, South China: implications for the genesis of porphyry copper mineralization. J. Petrol. 47, 119–144.
Wang, Q., Wyman, D.A., Zhao, Z.H., Xu, J.F., Bai, Z.H., Wiong, X.L., Dai, T.M., Li, C.F., Chu, Z.Y., 2007a. Petrogenesis of carboniferous adakites and Nb-enriched arc basalts in the Alataw area: northern Tianshan Range (Western China): implication for Phanerozoic crustal growth of the Central Asia Orogenic Belt. Chem. Geol. 236, 42–64.
Wang, Q., Wyman, D.A., Xu, J., Jian, P., Zhao, Z., Li, C., Xu, W., Ma, J., He, B., 2007b. Early Cretaceous adakitic granites in the Northern Dabie complex, central

China: implications for partial melting and delamination of thickened lower crust. Geochim. Cosmochim. Acta 71, 2609–2636.
Wang, Q., Wyman, D.A., Zhu, T., Feng, X., Zhang, Q., Zi, F., Chu, Z., 2008. Eocene melting of subducting continental crust and early uplifting of central Tibet: evidence from central-western Qiangtang high-K calc-alkaline andesites, dacites and rhyolites. Earth Planet. Sci. Lett. 272, 158–171.
Whitney, D.L., Evans, B.W., 2010. Abbreviations for names of rock-forming minerals. Am. Mineral. 95, 185–187.
Xu, J.F., Shinjio, R., Defant, M.J., Wang, Q., Rapp, R.P., 2002. Origin of Mesozoic adakitic intrusive rocks in the Ninzhen area of east China: partial melting of delaminated lower continental crust. Geology 12, 1111–1114.
Xu, W.L., Wang, Q.H., Wang, D.Y., Guo, J.H., Pei, F.P., 2006. Mesozoic adakitic rocks from the Xuzhou-Suzhou area, eastern China: evidence for partial melting of delaminated lower continental crust. J. Asian Earth Sci. 27, 230–240.
Zhu, D.C., Zhao, Z.D., Pan, G.T., Lee, H.Y., Kang, Z.Q., Liao, Z.L., Wang, L.Q., Li, G.M., Dong, G.C., Liu, B., 2009. Early cretaceous subduction-related adakite-like rocks of the Gangdese Belt, southern Tibet: products of slab melting and subsequent melt-peridotite interaction? J. Asian Earth Sci. 34, 298–309.